Doctor Thesis

Studies to unveiling the fundamental mechanisms on complex systems from DNA molecule to human

DNA 分子からヒトに至る複雑系に潜む基本原理を探る研究

Hikari Baba

馬場ひかり

Graduate School of Life and Medical Sciences,
Doshisha University

同志社大学大学院　生命医科学研究科

November, 2021

Table of Contents

List of Figure Caption

Fig. 2.10 CD spectra of calf thymus DNA in the absence and presence of AuNPs at different temperature conditions: (A) room temperature (without any heating); (B) 70 ℃; (C) room temperature (after heating).

Fig.3.1 Morphological change in the dried state for an aqueous solution containing glucose and starch. The weights of [Glucose]+[Starch] and [Water] were fixed at 20g and 8g, respectively. $\alpha(\mathrm{g/g}) = [Glucose]/([Glucose] + [Starch])$

Fig.3.2 ^{1}H NMR spectra of peeling film, bottom layer, glucose and starch (400 MHz, D6-DMSO, [Glucose] = 8g; [Starch] = 12g; [Water] = 8g, α = 0.4).

Fig.3.3 Schematic representation of the drying processes at different glucose contents (see Fig. 3.1). (a): cracking at a low glucose content; (b): peeling at a higher glucose content.

Fig.3.4 Numerical modeling of the time development of drying for an aqueous solution. (a) and (b) correspond to lower and higher glucose contents, respectively.

Fig.S3.1 Φ dependence of $D(\Phi)$. (a) and (b) are the effective diffusion constants depending on Φ, adapted in the present simulation. In (b), $D(\Phi)$ exhibits small negative value between 0.63 and 0.73.

Fig.4.1 Schematics of standing conditions. (a) Standing condition on the upright posture. (b) Standing on the condition of posture with legs as front and back. (c) Directions of X-Y axis, Front/Rear and Left/Right.

Fig. 4.2 Time-delay maps on the body fluctuations in the directions of the left/right and front/rear with the subject's eyes opened. Colors express the elapsed time.

Fig. 4.3 Time-delay maps on the body fluctuations in the directions of the left/right and front/rear with the subject's eyes closed. Colors express the elapsed time.

Fig. 4.4 Time-delay maps on the body fluctuations in the directions of the left/right and front/rear with the legs as front and back and the subject's eyes opened. Colors express the elapsed time.

Fig. 4.5 Time-delay maps on the body fluctuations in the directions of the left/right and front/rear with the legs as front and back and the subject's eyes closed. Colors express the elapsed time.

Chapter 1

General Introduction

As a part of living beings, the life phenomenon is very familiar to us. , However, it still is a mystery with many unexplained matters. Even many researchers have taken various approaches to understand life and gained a lot of knowledge, at present, it can not be said that the essence has been clarified.

For example, in the field of molecular biology, it is believed that all genetic information is contained in the DNA sequence. In recent years, due to rapid development in technology, we have finished decoding the entire base sequence of many organisms, including humans. However, can anyone really describe the entire spatiotemporal structure of life with one-dimensional information such as the sequences of only four types of bases? It is said that the base sequence encodes an amino acid sequence for making a protein and also plays a role in controlling it. That is everything that we understand now.

Furthermore, life beings create various cells with various roles by cell differentiation. All of their DNAs are all carrying the same information. It is essentially

unclear how to selectively read information from the exact same DNA to form organs with different functions and structures.

In addition, life is a system (non-equilibrium open system) that is constantly exposed to inflow and outflow of energy and substances. It is generally known that interesting phenomena such as nonlinear vibration, bifurcation, and chaos occur in a non-equilibrium open system. Such energy exchange has a very great effect on microscopic scale such as DNA and protein, and each molecule is constantly fluctuating violently. On the other hand, if we look at each organ or individual that is an aggregate of them on a macro scale, we can not see the effect of fluctuations. This is a cascade that is the exact opposite of the second law of thermodynamics, and it is very interesting to understand how to create a deterministic phenomenon from a large fluctuation. Ordering phenomena (fluctuations and precise patterns) that occur in such a chaotic system are inherent in phenomena on all length scales. To explore the formation of spatiotemporal order on various scales is essential to clarify the characteristics and dynamics of life.

Therefore, in this paper, I aim to quantify and model the order phenomenon on all length scales from the aspects of experiments and theoretical models.

In Chapter 2, I report the results of discovering the characteristic rhythm pattern inherent in single-molecule DNA on the order of nanometers to micrometers and evaluating the physical properties of DNA in a state close to a living body. The contents of this chapter are published in Publications [1].

In Chapter 3, I report the results of the transition phenomenon (centimeters order) of dry patterns caused by the mixing ratio of two substances with the same composition (high molecular weight starch and low molecular weight glucose) and the

results of modeling their patterns in a simple diffusion equation. The contents of this chapter are published in Publications [2].

In Chapter 4, I report the results of analyzing the characteristics inherent in the fluctuation of the body of a standing person from the viewpoint of time-reversal symmetry breaking. The contents of this chapter are published in Publications [3].

In Chapter 5, I give an overall summary and future prospects.

Chapter 2

Decorating a single giant DNA with gold nanoparticles

2.1 Introduction

Nanoparticles (NPs) have attracted considerable interest with regard to both their potential applications in medicine and basic understanding of biological systems. The evolution of nanoscience has led to the development of a wide variety of methods to fight cancer and image damaged organisms[1,2]. In gene therapy, DNA is transferred into the living cells of patients. Nevertheless, the principal challenge in the design of gene delivery systems lies in the carrier's ability to overcome different biological barriers and reach the target in an efficient manner[1,3,4]. Due to the limitations of a modified virus for this purpose, non-viral vectors (and particularly NPs) have become important[4]. On the other hand, the easy control of NPs' size and charge allows

mimicking proteins and other kinds of macromolecules and studying their effects in the DNA structure. For example, cationic nanoparticles have been used to study the DNA's wrapping or bending by electrostatic interaction with the purpose of simulating the chromatin-like structures at different levels of organization[5–7]. Not only the effect of the charge in the DNA structure can be studied throughout this method, but also the effect of the occupied volume by macromolecules, making nanoparticles an excellent tool for studying the crowding effect in living cells[6–8].

Among the many types of NPs, those with noble metal cores are especially popular due to their amazing optic properties[9] which gives rise to a whole new field involving the engineering and architecture of DNA-noble metal NPs conjugates[10–12]. Oscillation of the electron cloud of nanoparticles upon interaction with the electric field of light causes the colloidal system to absorb electromagnetic radiation, and, for noble metal NPs, this absorption is in the visible range[13]. This strong and broad band is called the Surface Plasmon Resonance (SPR) band and its characteristics depend on the physical properties of the NPs and the environment[13,14]. Among all existing nanoparticle types, gold nanoparticles (AuNPs) have enjoyed the greatest rise in popularity, despite the fact that silver nanoparticles display a stronger and narrower band than colloidal gold[15]. This is in no small part due to the inert nature and biocompatibility of gold[16], which allows for generating different structures with a wide range of properties according to the “construction block”[17–19]. DNA-AuNPs systems have received a large boost over the past few years, and the number of publications on this topic has grown exponentially[20]. This marked interest has been principally due to the versatile interactions between AuNPs and thiolated

oligonucleotides, which allow for the easy and selective functionalization of these colloids[20,21]. In addition, the nucleobases exhibit a strong tendency to interact with the AuNP surface, and each shows a different adsorption affinity[22]. In this way, appropriate oligonucleotide design could allow for the anchoring of short DNA molecules to a nanoparticle surface without the need for a sulfur bond. These adsorption processes enable, among many other applications, the detection of oligonucleotide hybridization upon the addition of salt, since non-complementary molecules tend to stick to the nanoparticle surface, increasing the colloid's charge and its stability against aggregation processes[23,24]. Consequently, studies about noble metal NPs and DNA have mainly focused on the interaction of single-stranded oligonucleotides with AuNPs, and much less is known about the interactions of these systems with long DNA molecules[25]. As a consequence of their predominant use as sensors, there has been little interest in the physical effects of AuNPs on DNA, including oligonucleotides. As an example, a recent study examined the influence of cationic colloidal silver on the DNA structure; the structural changes of the polymer depended on the nanoparticle concentration and charge, and partial strand separation was achieved[26].

In the present work, we report the formation of AuNP/DNA complexes by a novel and easy method involving giant DNA (T4-DNA; 166 kbp) and anionic AuNPs, without the need for any surface alteration. It should be noted that the procedure adopted in the present study is markedly different than those in studies using DNA as a template, where the nanoparticles' functionalization was required, either with cationic ligand to reach the interaction via electrostatic attraction with anionic phosphate groups[27,28] or using oligonucleotides to make the assembly by DNA hybridization

mechanism[11,29]. Besides we have focused our attention on the interaction of AuNPs with genome-sized giant DNA molecules because it is well known that the persistence length of double-stranded DNA molecules is around 170 bp (or 50 nm), so this implies that DNA below the size of kbp behaves as a stiff rod whereas giant DNA molecules above the size of several tens of kbp are regarded as semi-flexible polymer chains. Actually, giant DNA molecules with lengths on the order of 100 kbp undergo a large discrete transition, contrary to short DNA molecules which tend to aggregate without a folding transition[30,31]. In addition, changes in the higher-order structure of DNA are believed to be involved in the regulation of gene expression[32,33]. Furthermore, studies on the basic properties of giant DNA molecules are expected to shed light on the underlying mechanism of epigenetic phenomena[34]. Here we have evaluated and obtained the spring constant on genome sized DNA though the observation of fluctuating molecules. Although there have been so many studies on the measurements of the Brownian fluctuation of DNA molecules, these studies have failed to obtain the precise information on the intrachain fluctuation eliminating the influence of translational and rotational fluctuations[30,31]. The procedure developed here to obtain the spring constant means the base for future studies in the higher order structure of genome sized DNA by the interaction with different kind of molecules, for example, anticancer agents.

2.2 Experimental Methods

2.2.1 Materials

Hydrogen tetrachloroaurate(III) trihydrate was purchased from Sigma-Aldrich (St. Louis, MO, USA), and trisodium citrate was from Alfa Aesar (Haverhill, MA, USA); they were used without further purification. All chemicals were of analytical reagent grade. Solutions were prepared with deionized water with a conductivity of less than 10^{-6} S m^{-1}.

T4 GT7 phage DNA (166 kbp with a contour length of 57 μm) was purchased from Nippon Gene Co., Ltd. LTP (Toyama, Japan). Calf thymus DNA (CT DNA: 8–15 kbp) was purchased from Sigma-Aldrich. The fluorescent dye GelGreen was obtained from Biotium (Fremont, CA, USA). The antioxidant 2-mercaptoethanol (2-ME) was purchased from Wako Pure Chemical Industries (Osaka, Japan).

2.2.2 Synthesis and characterization of gold nanoparticles

Citrate-capped AuNPs with an average size of around 15 nm were prepared according to a variation of Turkevich's method, by reduction of a gold complex in a liquid phase[35]. 97 ml of $HAuCl_4$ (0.01%) was heated under reflux at 90 ºC, and then, at this temperature, 3 ml of tri-sodium citrate (38.8 mM) was added. Heating under reflux was continued for an additional 10 minutes, during which time the color changed to deep red. The solution was then left stirring at room temperature for 24 hours.

In the UV-Vis absorption spectra, the absorption maximum wavelength was located at 520 nm. This wavelength is similar to that obtained in previous studies on AuNPs with a size of *ca.* 15 nm, making it possible to estimate the extinction coefficient: $\varepsilon = 3.9 \times 10^8\ M^{-1}cm^{-1}$[36]. The concentration can be obtained by applying the Lambert–Beer law: $[AuNPs] = 3.9 \times 10^{-9}$ M.

2.2.3 Preparation of assemblies of single DNAs with AuNPs

10 µl of T4 DNA solution (10 µM) was added to 790 µl of Tris-HCl buffer solution (pH 7.5). This sample was placed in a water bath at 60 ºC for 10 minutes. Next, without moving the bath container, 200 µl of a 15 nm AuNP dispersion was added to give final concentrations of [DNA] = 0.1 µM and [AuNP] = 0.8 nM. The sample was kept in the bath for an additional 5 minutes, and then left to cool to room temperature (24 ºC). A DNA solution at the same concentration and treated in the same way as the sample was used as a control. Another sample with its respective control but without any heating was also prepared.

2.2.4 Fluorescence microscopy (FM) measurements

2-ME and the dye GelGreen were added to 950 µl of the sample, with final concentrations of 4% (v/v) and 5 µM, respectively. 2-ME was used as a free-radical scavenger to reduce fluorescent fading and light-induced damage of DNA. GelGreen was added to visualize individual DNA molecules by FM. In a previous work, we

confirmed that GelGreen has a negligible effect on the conformation of DNA molecules at the concentrations used in observations by fluorescence microscopy[37]. Single-DNA observations were performed with an Axiovert 200 inverted fluorescence microscope (Carl Zeiss, Oberkochen, Germany) equipped with a 100× oil-immersion objective lens and fluorescent illumination from a mercury lamp (100W) via a filter set (Zeiss-10, excitation BP 450–490; beam splitter FT 510; emission BP 515–565). Images were recorded onto a DVD at 30 frames per second with a high-sensitivity EBCCD camera (Hamamatsu Photonics, Shizuoka, Japan) and analyzed with an image-analysis software, Cosmos32 (Library Co., Ltd., Tokyo, Japan).

2.2.5 Transmission electron microscopy (TEM) measurements

For TEM examinations, a single drop (10 µl) of the sample was placed on a carbon film-coated copper grid, which was then left to dry in air for several hours at room temperature. TEM observations were performed with an energy filtered-TEM JEM2100F electron microscope (JEOL, Tokyo, Japan) at 200 kV. The samples were analyzed at different magnifications (4k, 6k, 8k, 10k, 12k, 15k, 40k, 100k, 300k), and then magnified 30-fold with a CCD camera (Olympus, Tokyo, Japan).

2.2.6 UV-visible spectra

AuNP spectra were recorded from 400 to 800 nm with a Cary 500 spectrophotometer (Agilent, Santa Clara, CA, USA). The path length of the quartz

cuvette was 1 cm. Experiments were carried out under different temperature conditions at a fixed colloidal gold concentration ([AuNPs] = 8×10^{-10} M) in the absence and presence of CT DNA ([DNA] = 5×10^{-5} M).

2.2.7 Circular dichroism (CD) spectra

Electronic CD spectra were recorded in a Mos-450 spectropolarimeter (Bio-Logic, Seyssinet-Pariset, France). A standard quartz cell with a path length of 1 cm was used. The spectra were expressed in terms of ellipticity. Scans were taken from 230 nm to 320 nm for the intrinsic region of the DNA. For each spectrum, 5 runs were averaged at different temperatures. All the spectra were obtained with a fixed concentration of CT DNA ([DNA] = 5×10^{-5} M), both in the absence of and at a fixed concentration of AuNPs ([AuNPs] = 8×10^{-10} M).

2.3 Results and Discussion

In several preliminary experiments on the interaction of AuNPs with giant DNA molecules, we noticed that most AuNPs tend to effectively bind DNA molecules under mild warming at around 60–70 ºC. To avoid the effect of the melting transition on double-stranded DNA, we chose a warming temperature at 60 ºC and observed the obtained assemblies by several different methods. Here, we present the results of observations of complexes between DNA and AuNPs, by comparing the results for samples after warming at 60 ºC with control specimens prepared at 24 ºC (room temperature). Fig. 2.1 exemplifies images of T4 DNA (166 kbp) observed by fluorescence microscopy (FM). Fig. 2.1A and B correspond to control DNA samples in the absence of AuNPs, before and after warming at 60 ºC, respectively. In both cases, elongated DNA molecules exhibit translational and intrachain fluctuation as Brownian motion in the bulk aqueous solution. The observations at room temperature (24 ºC) are similar to those reported in previous studies[7,38]. With the addition of AuNPs to DNA solution at room temperature (Fig. 2.1C), DNA molecules remain in an elongated conformation. In the sample after warming (Fig. 2.1D), DNA molecules exhibit a rigid conformation, *i.e.*, almost no intrachain fluctuation is observed except for fluctuating translational and tumbling motions. Additionally, bright dots are arranged along a single DNA molecule.

To evaluate the degree of intramolecular Brownian motion, we analyzed fluctuation on fluorescence images of single DNA molecules before and after decoration by AuNPs. The red line in Fig. 2.2 shows the time-dependent fluctuation of

the long-axis length for a T4 DNA molecule after warming in the presence of AuNPs. The blue line shows the fluctuation for a natural DNA molecule in the absence of AuNPs. It is apparent that the single DNA in an assembly with AuNPs after gentle warming exhibits a rather stiff structure with a significant decrease in intrachain fluctuation. Interestingly, a single-DNA assembly is essentially the same size as that of native DNA without AuNPs. It has been well established[30,39] that many chemical agents, such as polyamines, cationic surfactants, crowding solvable polymers, *etc.*, cause the tight compaction of giant DNA molecules. Thus, the effect of AuNPs on the higher-order structure of DNA is rather specific, and leads to a marked change in fluctuation by maintaining the conformation without compaction/condensation.

Next, we evaluated the autocorrelation $C(\tau)$ from the time-dependent fluctuation of the long-axis length, $L(\tau)$:

$$C(\tau) = \langle L(\tau) - \bar{L}\rangle\langle L(0) - \bar{L}\rangle \tag{2.1}$$

where $\bar{L}$ is the time-average of the long-axis length.

Based on a theoretical model of thermal fluctuation under a harmonic potential, the autocorrelation function is represented as in eqn(2.2) to a reasonable approximation[40]:

$$C(\tau) \sim \frac{k_B T}{k} e^{-\gamma\tau} cos\omega\tau \tag{2.2}$$

where k_B is the Boltzmann constant, T is absolute temperature, k (N/m) is the spring constant, γ (sec^{-1}) is a damping coefficient and ω is angular frequency. The spring constant k can be evaluated from the initial value of the autocorrelation function, $C(\tau = 0) \equiv C(0)$, by using the relationship $k \approx \frac{k_B T}{C(0)}$. From the vertical axis at $\tau = 0$ in

Fig. 2.3, $C(0)$ is calculated as 0.46 ± 0.09 and 0.034 ± 0.007 μm^2 for natural and Au-decorated DNA, respectively. Thus, the spring constants k of natural DNA and Au-decorated DNA are $k_0 = (8.9 \pm 1.8) \cdot 10^{-9} N/m$ and $k_{A_u} = (1.2 \pm 0.3) \cdot 10^{-7} N/m$, respectively, by taking $T \approx 300$ K. In other words, the spring constant of Au-decorated DNA is *ca.* 13 times larger than that of natural DNA. Next, we deduce physico-parameters from the fitting curves based on eqn (2.2), as in the broken lines in Fig. 2.3. The damping coefficients for natural and Au-decorated DNAs are thus evaluated to be $\gamma_0 = 1.1 \pm 0.3\ sec^{-1}$ and $\gamma_{Au} = 5 \pm 2\ sec^{-1}$, respectively. As for the angular frequencies, we found that $\omega_0 = 3.2 \pm 0.7\ rad/sec$ and $\omega_{Au} = 24 \pm 6\ rad/sec$, respectively. From the fundamental characteristics of a harmonic oscillator with spring constant k, we assume the relationship to be $k \propto \omega^2$. Although the experimental error for the angular frequency of Au-decorated DNAs is rather large, the relationship of $k \propto \omega^2$ seems to be supported by the data obtained from the analysis of the autocorrelation function. Recently, there has been an increasing number of experimental trials to measure the elasticity of DNA by use of the experimental technique of laser tweezers. Unfortunately, most of the current studies reported the observed spring constant for short DNA molecules smaller than several kbp, which is due to the technical difficulty of measuring the elastic properties of giant DNA molecules. Instead, we can roughly estimate the Hooke spring constant for long DNA based on a simple theoretical prediction[41-43]:

$$k \sim {k_B T}/{l_p L} \tag{2.3}$$

where l_p and L are the persistence length and contour length, respectively. For the T4 DNA used in the present study, we can estimate $l_p = 50$ nm and $L = 57$ μm. Thus, we can expect that the spring constant of T4 DNA would be several pN/m (= $10^{-9}N/m$), corresponding to the values obtained from the analysis of the fluctuation of single DNA molecules. The spring constant and damping coefficient's rise can be attributed to several factors. Amongst them, the increase of the bending stiffness with the binding of AuNPs, the increase of the self-avoiding volume effect, and/or the steric and electrostatic repulsions between nanoparticles are some of the most important. If we consider the DNA molecule as a semi-flexible chain, the assembly of colloidal gold involves attaching a (comparatively) huge and rigid sphere to the biopolymer chain; in turn, the DNA segments which are interacting with it also get increasingly stiff. One of the factors that determines DNA stiffness is the negative charge of the chain, since electrostatic repulsion forces cause the phosphate groups to be separate. The presence of anionic nanoparticles in a DNA fragment implies an increase of the local charge in that point and forces these fragments to acquire more rigid conformations to minimize the aforementioned repulsions.

As for the DNA–AuNP assemblies generated by mild warming, by visual inspection there was no apparent color change for the sample solution before and after warming, suggesting that the AuNPs exhibit negligible aggregation. To check the solution conditions including aggregation in a quantitative manner, we carried out UV-Vis absorption measurements. Fig. 2.4 shows the SPR band of AuNPs in the presence and absence of DNA at different stages of the process, which reveals essentially the same absorption spectrum before and after warming. Here, we show the spectrum for

the DNA – AuNP assembly after warming at 70℃, to show the minimum effect of warming on plasmon absorption. (There was no detectable difference between samples after warming at 60 ℃ or 70 ℃.) It is well known that the SPR band shifts to a higher wavelength when the size of AuNPs becomes larger due to electric field coupling. In addition, it has been reported that symmetry-breaking of spherical Au particles as the result of tight contact between them causes a quadrupolar absorption band at around 600 nm[44].

As mentioned above regarding the measurements by fluorescence microscopy and UV-Vis spectroscopy, we have shown that decorated individual giant DNA molecules are soluble in solution by avoiding aggregation and precipitation. However, the resolution of fluorescence microscopy is relatively low and is on the order of 0.5 μm. To obtain information on the detailed morphology of individual giant DNA decorated with AuNPs, we performed TEM observations. Fig. 2.5A shows AuNPs prepared in the absence of DNA, indicating the presence of randomly dispersed particles absorbed on a carbon film. Fig. 2.5B shows the results for a mixture of T4 DNA and AuNPs without warming, revealing that, while nanoparticles tend to attach to the DNA chain, a certain proportion remain unbound and are dispersed on the solid substrate. Interestingly, all of the particles bound to the DNA skeleton and resulted in greater density along the DNA chain (see Fig. 2.5C), in contrast to the sample prepared at room temperature. In accordance with the experimental results by fluorescence microscopy, the fully decorated sample prepared by mild warming exhibits only slight shrinkage compared to that prepared without warming. A more detailed comparison of the warmed and un-warmed samples is presented in the ESI (see Fig. 2.6-2.8). Interestingly, the obtained

structures are different than what would be obtained if the biopolymer acted as a mere template (DNA metallization), where the assembly of metallic nanoparticles would be more branched and ordered, or could even behave as a nanowire[45,46]. In addition, the morphology observed by FM is similar to that observed by TEM, despite the large difference in spatial resolution in addition to the difference in the observation conditions, *i.e.*, in solution or dry on a solid substrate (see Fig. 2.9). On the other hand, as mentioned above, there was no apparent difference in the UV-visible spectrum or the SPR band, which implies that aggregation among AuNPs is almost negligible or that the interaction between neighboring colloids along the DNA molecule is relatively weak.

In any case, the differences between Fig. 2.5B and C show extremely different behaviors depending on the heating process. These differences in structure are due to enhanced DNA–AuNP interactions in the complexes formed upon warming. A possible explanation is that there is a partial separation of T4 DNA during the heating process which causes a loss of DNA stiffness and further exposes the bases to the gold surface; for this reason, the aforementioned complex structures are not observed in the unheated sample. The interaction way of DNA molecules with citrate capped AuNPs has been extensively studied, being established through the base fragments[22,47–50]. In fact this interaction is so strong that it can break the hydrogen bond of base pairs in oligonucleotides, although that was observed with 5 nm AuNPs and not for 15 nm[48]. On the other hand, the phosphate groups of DNA molecules only interact when the colloidal gold has positive charge, due to electrostatic attractive forces, and it is noteworthy that the interaction is with the cationic functional group and not with the gold surface[5,51,52]. It has also be considered that at room temperature the AuNPs and

DNA molecules are inclined to be distant (due to they present the same charge) and therefore the binding is rather difficult[24,53]. As the temperature increases the thermal fluctuation too, so that the chances to collide of the AuNPs with DNA molecules are higher, being possible surpassing the energy barrier which avoids their approximation. In addition the partial denaturation of DNA can happen at higher temperatures, so the exposition of DNA's bases to the outside is viable and the interaction between bases and AuNPs does not need to overlap the repulsion electrostatic energy. Anyway, more studies are necessary to understand the mechanism that provokes an increase in the interaction between T4 DNA and anionic AuNPs at higher temperature.

Finally, to check if these interactions provoke changes in the secondary structure of DNA, the effects of temperature and the presence of NPs on the circular dichroism (CD) spectra of DNA were studied. Fig. 2.10A shows CD spectra for the samples at room temperature. The addition of AuNPs induces a slight decrease in the intensity of the positive band, although the basic character of the B-structure is preserved. An isosbestic point also appears over 258 nm, as has been previously observed for anionic nanoparticles and large DNA chains[53]. This small conformational change does not involve an opening of the double helix due to the nanoparticles; the negative band does not decrease in intensity, which would correspond to a loss of helicity of the DNA, and the crossover point does not change, while Dias and coworkers found that for melting processes, a 3 nm shift could be expected[54]. Even at 70 ℃, the essential feature characteristic to the B-form remains (see Fig. 2.10B), accompanied by a small decrease in the band height, suggesting the induction of a helix-coil transition at some portion of DNA.

Although no significant changes in DNA structure are observed at room temperature or adding AuNPs at 70 ℃, this is not the case at room temperature after heating (see Fig. 2.10C): an important decrease of intensity of the positive band (around 20%) consisting in the DNA compaction appears. Some authors have attributed these changes to bending phenomena[55], which are associated with small losses of π-stacking interactions and helicity. The same phenomenon has been described working with functionalized cationic gold nanoparticles and 37-residue oligonucleotides (see Fig. 2 in the ref. [5]). However in this case the DNA compaction took place by electrostatic interaction between negative charge of phosphate groups with the positive charge of the nanoparticle surface. This fact implies that not only a marked decrease intensity at 280 nm is present in the circular dichroism of DNA: it is coupled with a shift in the maximum wavelength. This point is not observed in the present study and cannot be concluded a total conversion of denatured double strand unlike the study carried out by Goodman and collaborators[5]. However, at no stage of the process do the DNA molecules show a conformation being largely and remarkably different from the B-form, suggesting that the secondary structure of DNA remains almost same as that before the decoration with AuNPs.

2.4 Conclusions

In the present article, successful decoration of a giant DNA molecule with AuNPs through the simple procedure of mild warning was described. Upon such decoration, the DNA molecule becomes stiffer while retaining an elongated conformation. On the other hand, there is no apparent change in the surface plasmon resonance of AuNPs, suggesting that they are dispersed, rather than aggregated. Electron microscopy observations support such dispersed positioning. In addition, it was confirmed that the secondary structure of DNA stays mostly as in the B-form after AuNP decoration. Further studies will be needed to gain a basic understanding of the structure and properties of AuNP-decorated giant DNA, and also to develop and optimize DNA–AuNPs complexes for practical applications in medicine.

2.5 Acknowledgements

We thank Miwako Toda for her assistance with obtaining TEM images, and Aila Jimenez-Ruiz (ailjimrui@alum.us.es) for help in revising English usage throughout this manuscript. This work was nanced by the Spanish Ministerio de Economia y Competitividad (MinECo), CTQ2016-78703-P (AEI/FEDER, UE), by the V Plan Propio Grupos Emergentes (V Own Gran Plan for Emerging Groups) of the Universidad de Sevilla, and by the OTRI (2010/00000762). We also thank Universidad de Sevilla for a predoctoral grant for the V-Plan Propio de Investigaci´on (VPPI-US). This work was partially supported by JSPS KAKENHI Grant Numbers 15H02121 and 25103012.

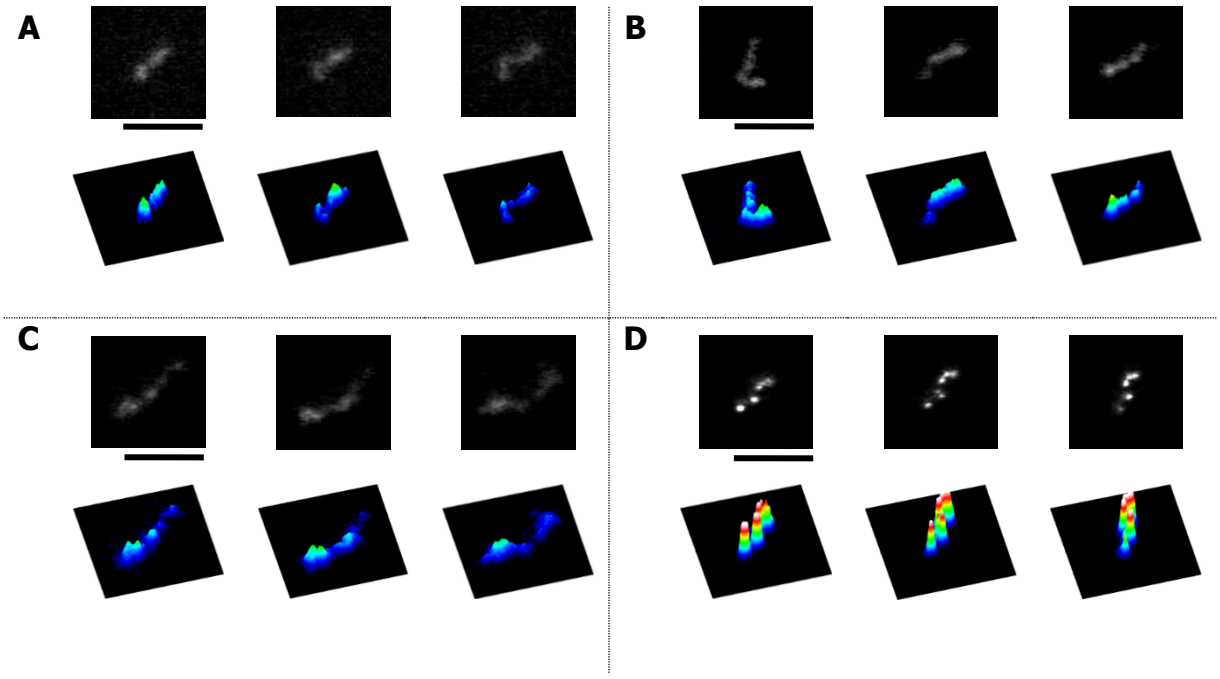

Figure 2.1 Real-time monitoring of single T4 DNA molecules in bulk solution as observed by fluorescence microscopy (at room temperature, 24 ºC). The time-interval between neighboring frames is 0.5 sec. A) In the absence of AuNPs without warming; B) in the absence of AuNPs after warming at 60 ºC for 15 min; C) in the presence of AuNPs without warming; D) in presence of AuNPs after warming at 60 ºC for 15 min. Corresponding quasi-three-dimensional (3D) images indicating the profiles of the fluorescence intensity distribution are also shown. The scale bar is 5 μm.

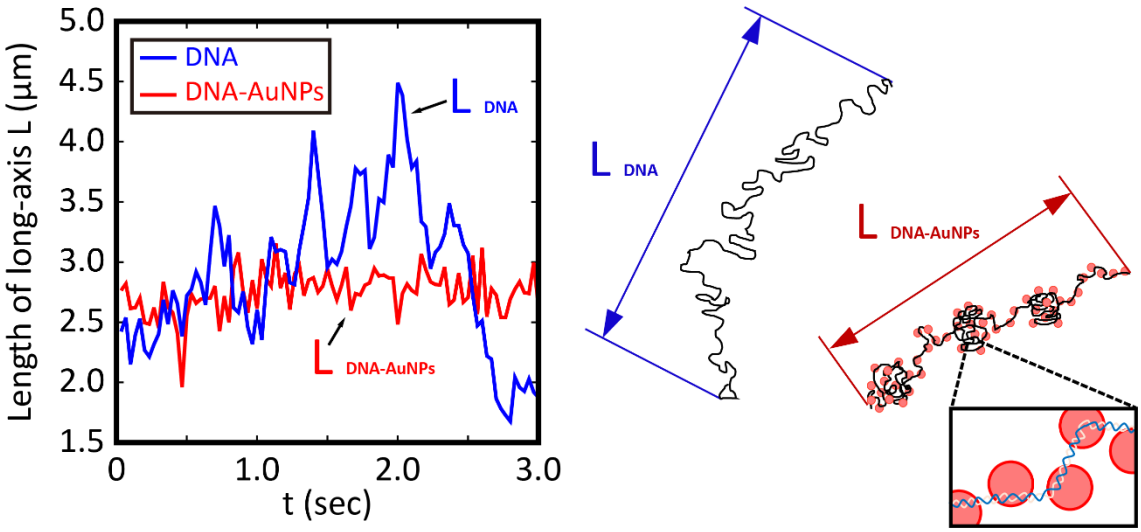

Figure 2.2 Time dependent change in the long-axis length of T4 DNA molecules without and with attachment to AuNPs as depicted by blue and red lines, respectively. The blue and red lines correspond to the samples in Figure 2.1 B) and D), respectively. Both measurements were performed at room temperature after warming at 60 ºC for 15 min. The blue line shows the time trace for DNA without AuNPs, and the red line shows that for the AuNP-DNA assembly. For convenience, schematic illustrations of the conformations are shown on the right side.

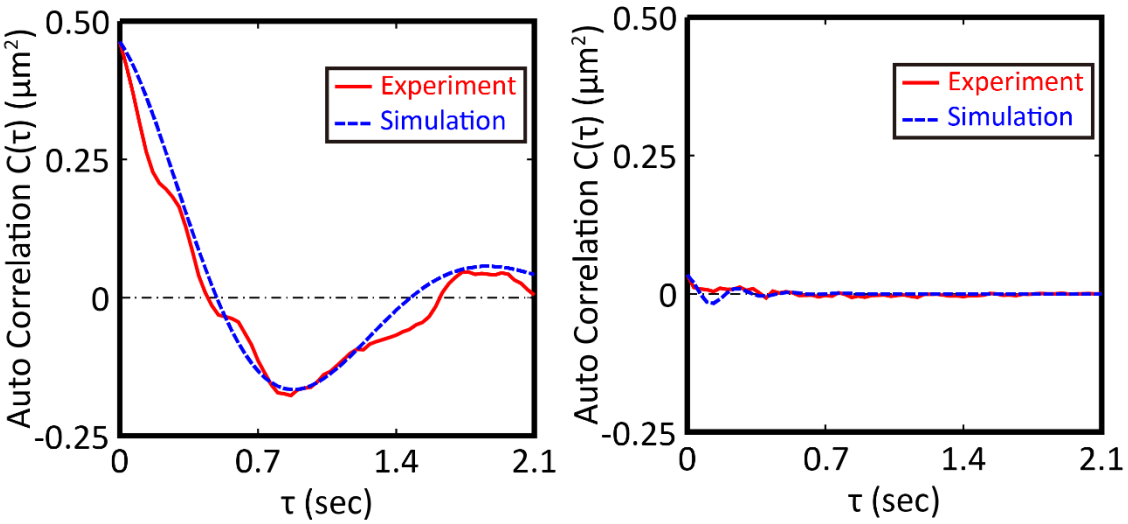

Figure 2.3 Autocorrelation function for the time-dependent fluctuation given in Figure 2.2. The fitting curve was depicted based on eq.(2.2). The left picture is the auto correlation function for DNA molecules in the absence of colloidal gold while that on the right is for DNA molecules decorated with gold nanoparticles.

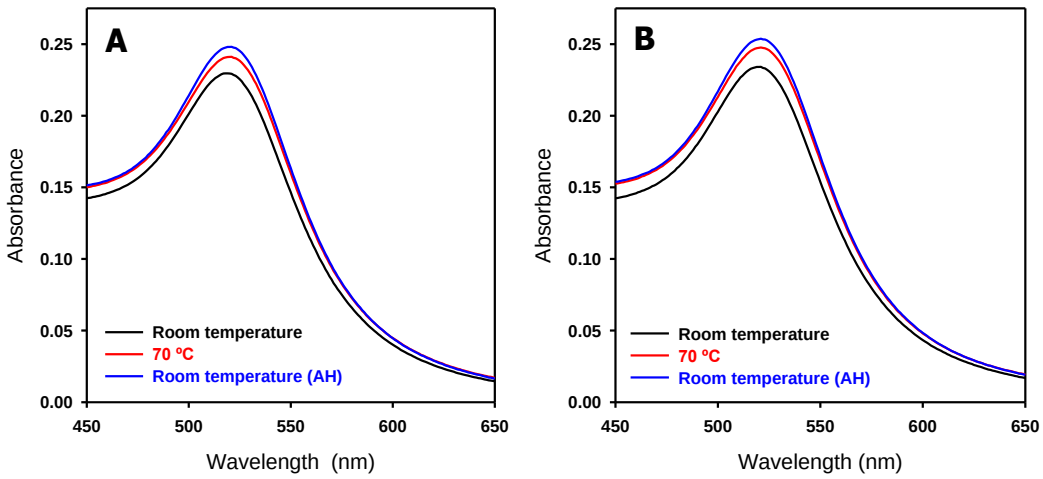

Figure 2.4 UV-Vis absorption spectra of AuNPs in the absence (A) and presence (B) of calf thymus DNA under different conditions: room temperature, 70 ºC and room temperature after the warming procedure (AH, after heating).

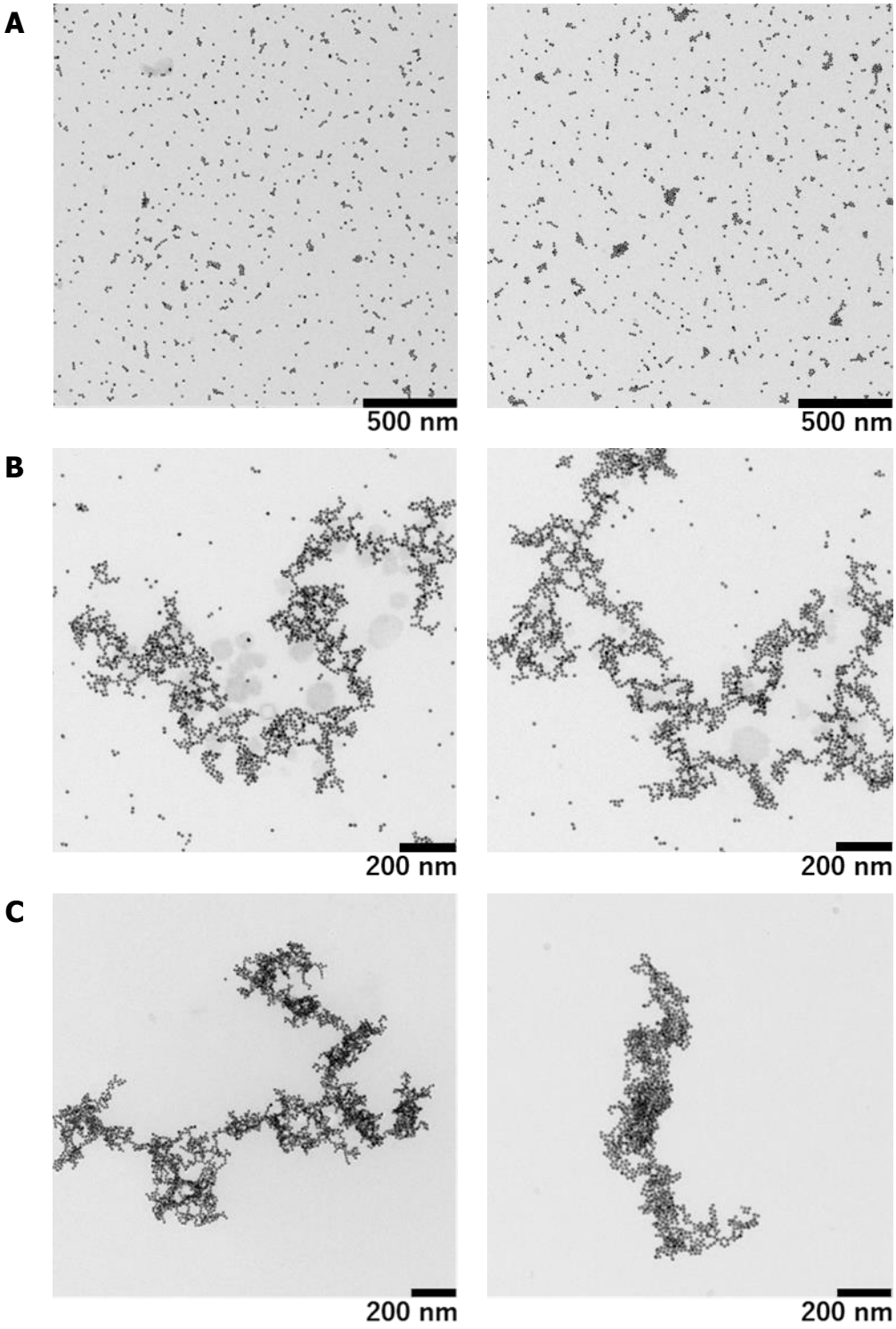

Figure 2.5 A) TEM images of dispersed gold nanoparticles at 4×10^{-9} M. B) TEM images of nanoparticles in the presence of T4 DNA; [AuNPs] = 0.8 nM; [DNA] = 1 μM. C) TEM images of nanostructures formed by heating a solution of [AuNP] = 0.8 nM and [DNA] = 1 μM.

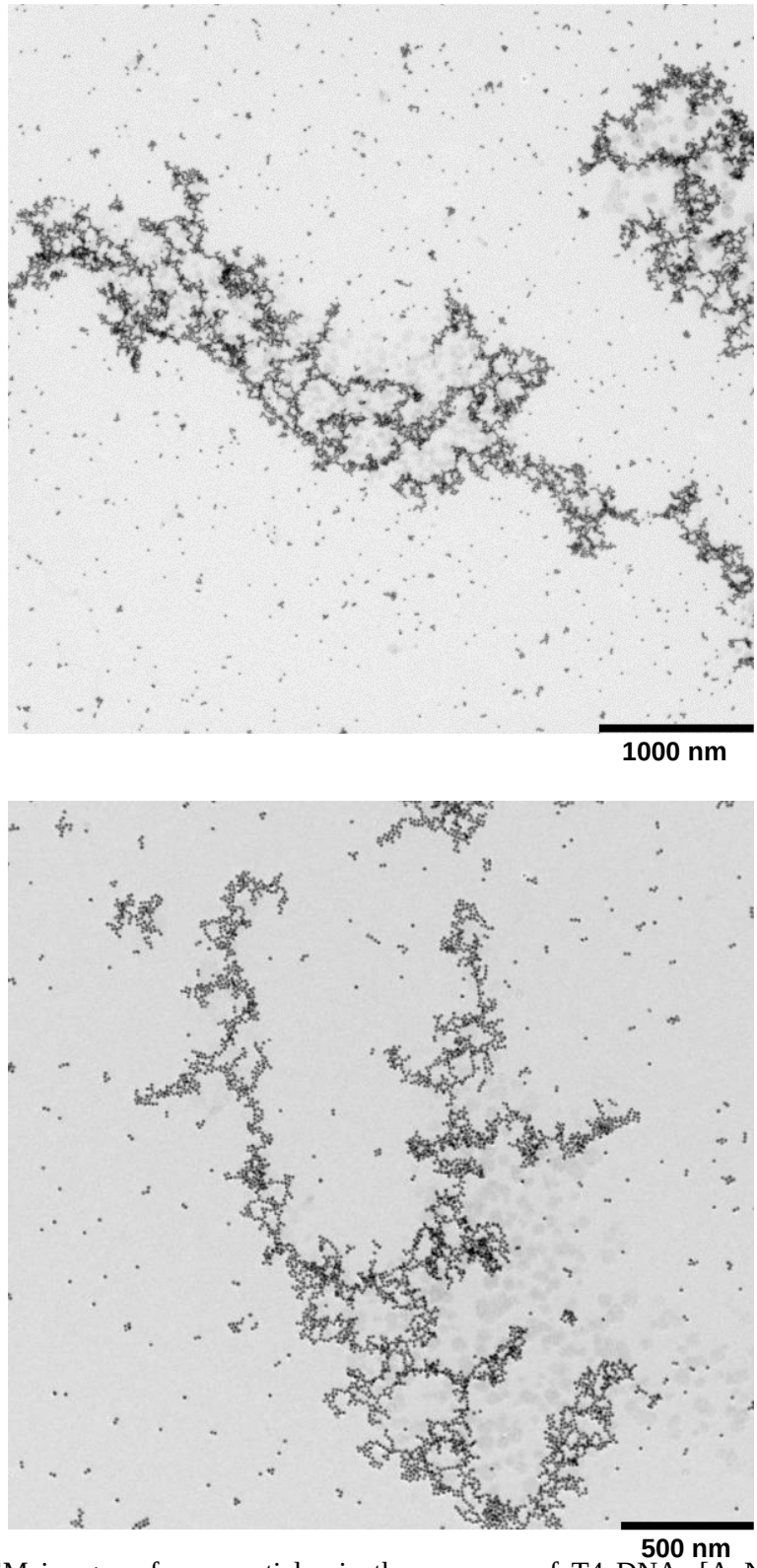

Figure 2.6 TEM images of nanoparticles in the presence of T4 DNA; [AuNPs] = 0.8 nM; [DNA] = 1 μM.

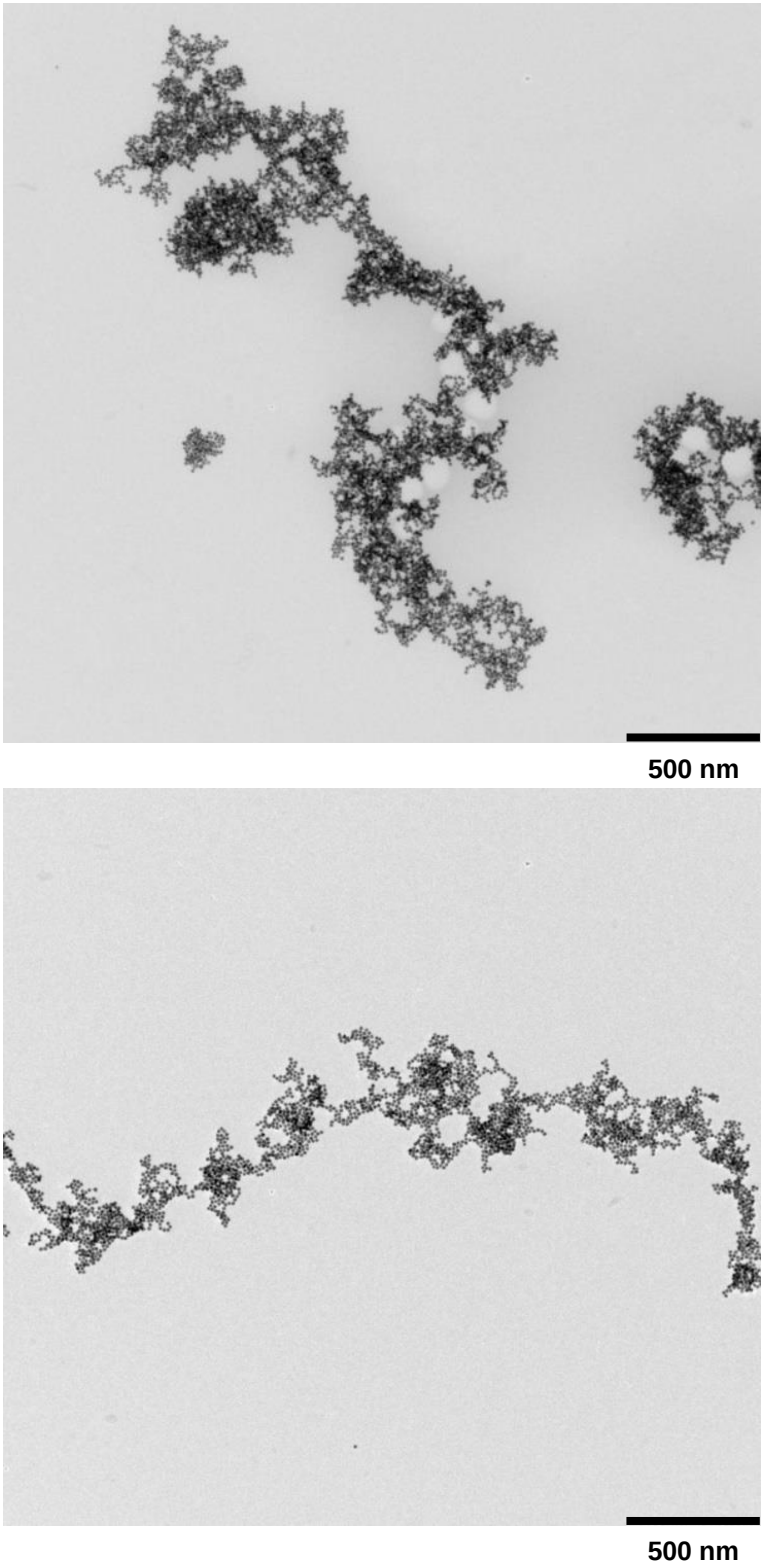

Figure 2.7 TEM images of nanostructures formed by heating a solution of [AuNP] = 0.8 nM and [DNA] = 1 μM.

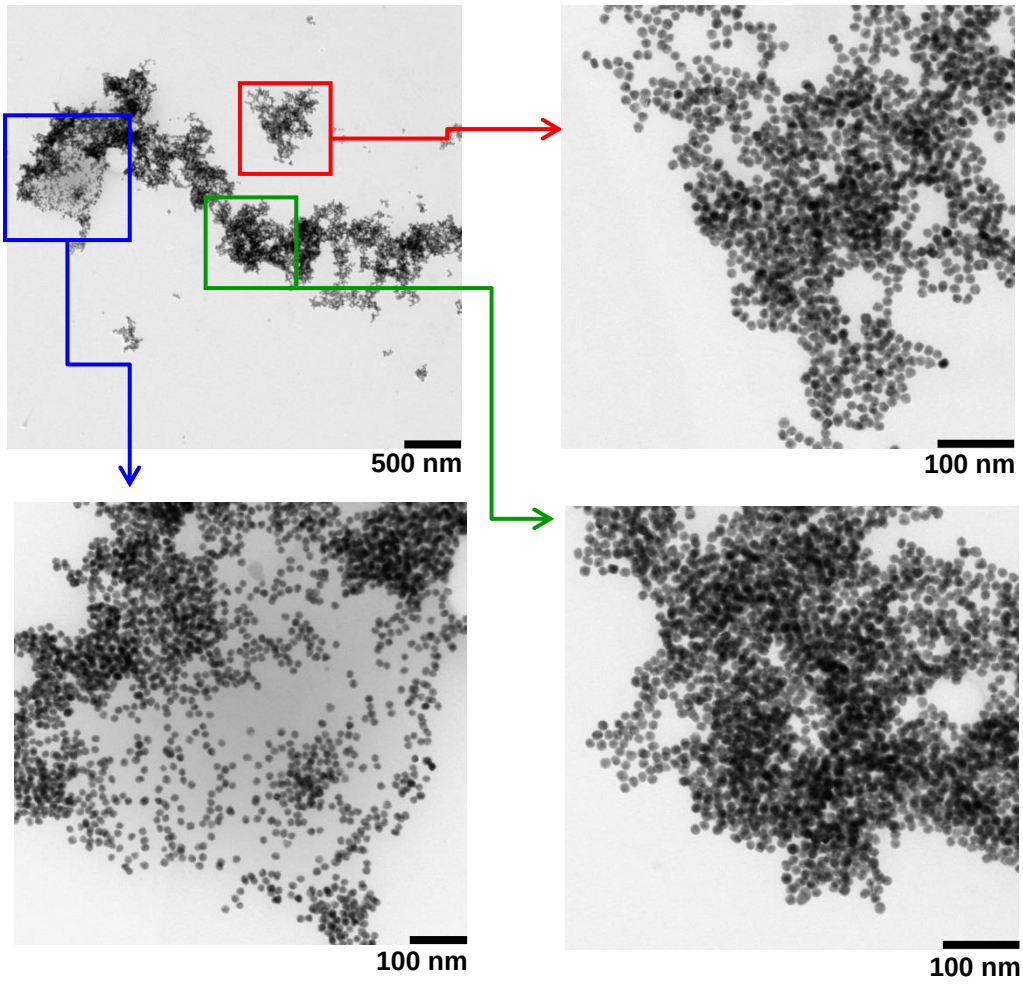

Figure 2.8 TEM images of nanostructures formed by heating a solution of AuNP (0.8 nM) and T4 DNA (1 µM). The amplified images show the accumulation of nanoparticles in various zones of the structure.

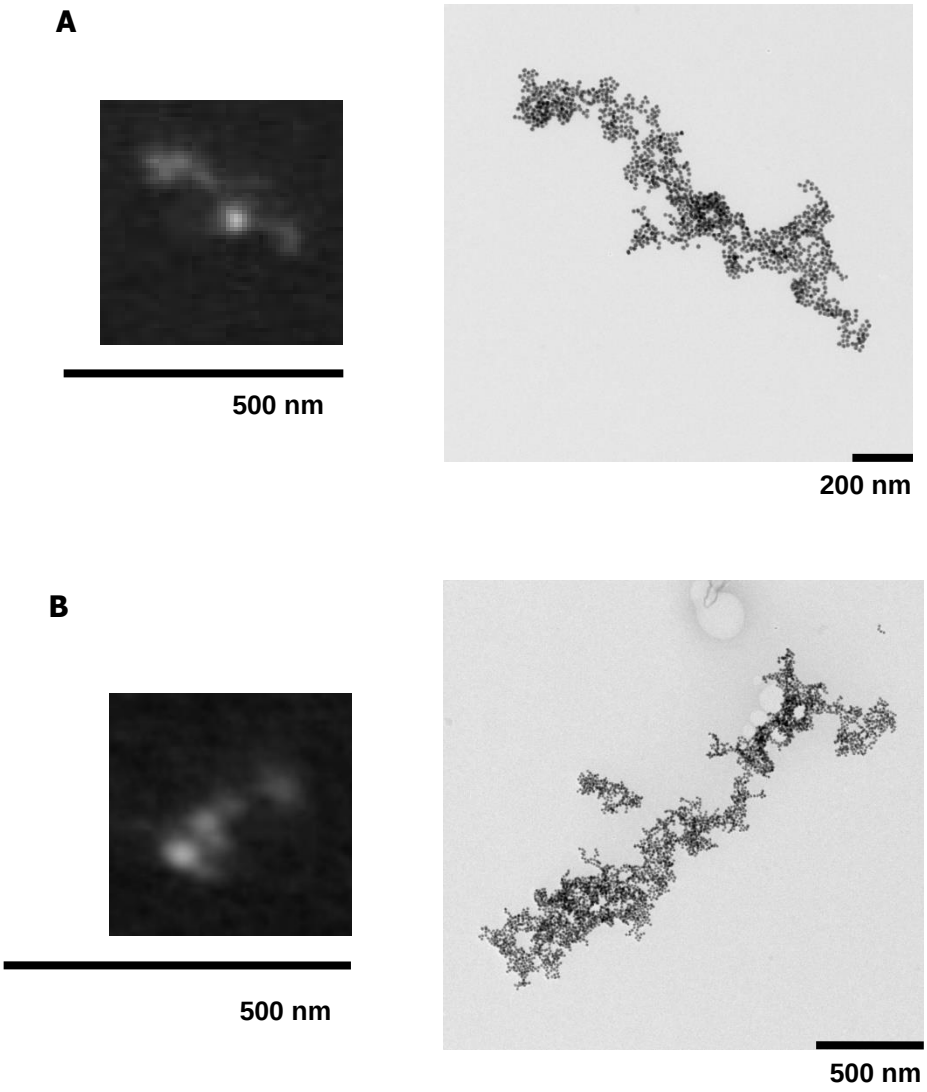

Figure 2.9 FM and TEM images of apparently similar nanostructures formed by heating a solution of AuNPs and T4 DNA.

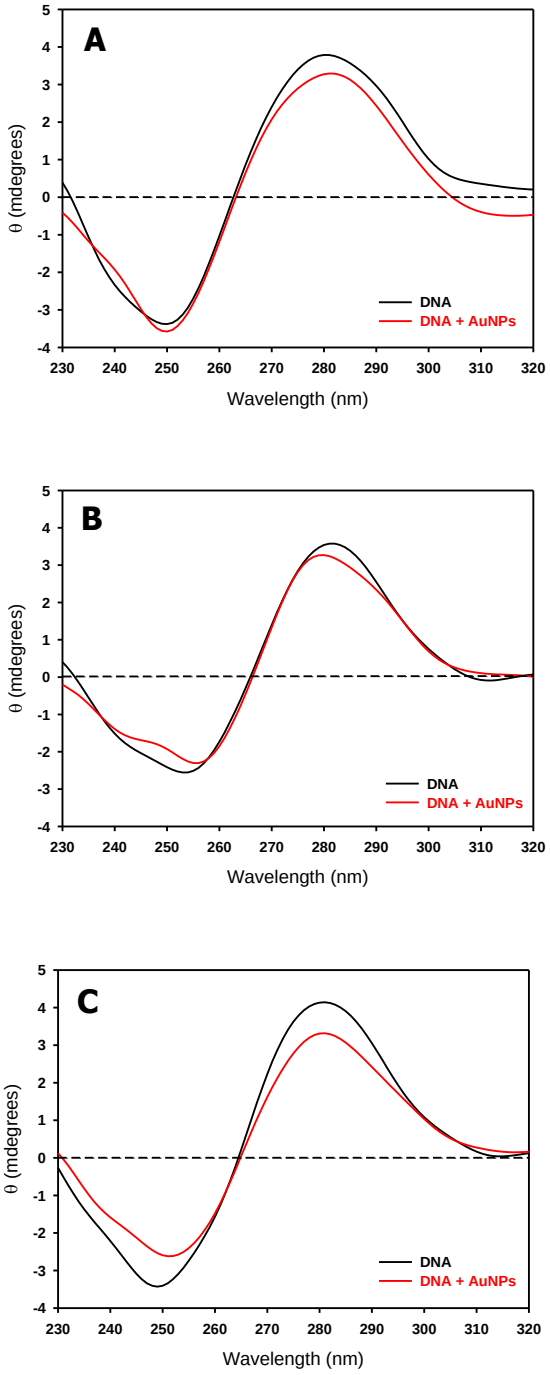

Figure 2.10 CD spectra of calf thymus DNA in the absence and presence of AuNPs at different temperature conditions: A) room temperature (without any heating); B) 70 ºC; C) room temperature (after heating).

References

[1] Pelaz, B., Alexiou, C., Alvarez-Puebla, R. A., Alves, F., Andrews, A. M., Ashraf, S., Balogh, L. P., Ballerini, L., Bestetti, A., Brendel, C., Bosi, S., Carril, M., Chan, W. C. W., Chen, C., Chen, X., Chen, X., Cheng, Z., Cui, D., Du, J., Dullin, C., Escudero, A., Feliu, N., Gao, M., George, M., Gogotsi, Y., Grünweller, A., Gu, Z., Halas, N. J., Hampp, N., Hartmann, R. K., Hersam, M. C., Hunziker, P., Jian, J., Jiang, X., Jungebluth, P., Kadhiresan, P., Kataoka, K., Khademhosseini, A., Kopeček, J., Kotov, N. A., Krug, H. F., Lee, D. S., Lehr, C.-M., Leong, K. W., Liang, X.-J., Ling Lim, M., Liz-Marzán, L. M., Ma, X., Macchiarini, P., Meng, H., Möhwald, H., Mulvaney, P., Nel, A. E., Nie, S., Nordlander, P., Okano, T., Oliveira, J., Park, T. H., Penner, R. M., Prato, M., Puntes, V., Rotello, V. M., Samarakoon, A., Schaak, R. E., Shen, Y., Sjöqvist, S., Skirtach, A. G., Soliman, M. G., Stevens, M. M., Sung, H.-W., Tang, B. Z., Tietze, R., Udugama, B. N., VanEpps, J. S., Weil, T., Weiss, P. S., Willner, I., Wu, Y., Yang, L., Yue, Z., Zhang, Q., Zhang, Q., Zhang, X.-E., Zhao, Y., Zhou, X. & Parak, W. J. "Diverse Applications of Nanomedicine". *ACS Nano* **11**, 2313-2381 (2017).

[2] Wolfbeis, O. S. "An overview of nanoparticles commonly used in fluorescent bioimaging". *Chemical Society Reviews* **44**, 4743-4768 (2015).

[3] Riley, M. K. & Vermerris, W. "Recent advances in nanomaterials for

gene delivery—a review". *Nanomaterials* **7**, 94 (2017).

[4] Yin, H., Kanasty, R. L., Eltoukhy, A. A., Vegas, A. J., Dorkin, J. R. & Anderson, D. G. "Non-viral vectors for gene-based therapy". *Nature Reviews Genetics* **15**, 541-555 (2014).

[5] Goodman, C. M., Chari, N. S., Han, G., Hong, R., Ghosh, P. & Rotello, V. M. "DNA - binding by functionalized gold nanoparticles: mechanism and structural requirements". *Chemical biology & drug design* **67**, 297-304 (2006).

[6] Nash, J. A., Singh, A., Li, N. K. & Yingling, Y. G. "Characterization of nucleic acid compaction with histone-mimic nanoparticles through all-atom molecular dynamics". *ACS nano* **9**, 12374-12382 (2015).

[7] Zinchenko, A. A., Sakaue, T., Araki, S., Yoshikawa, K. & Baigl, D. "Single-chain compaction of long duplex DNA by cationic nanoparticles: modes of interaction and comparison with chromatin". *The Journal of Physical Chemistry B* **111**, 3019-3031 (2007).

[8] Zinchenko, A. "DNA conformational behavior and compaction in biomimetic systems: Toward better understanding of DNA packaging in cell". *Advances in colloid and interface science* **232**, 70-79 (2016).

[9] Quinten, M. *Optical properties of nanoparticle systems: Mie and beyond*. (John Wiley & Sons, 2010).

[10] Capek, I. *DNA Engineered Noble Metal Nanoparticles: Fundamentals and State-of-the-Art of Nanobiotechnology*. (John Wiley & Sons, 2015).

[11] Storhoff, J. J. & Mirkin, C. A. "Programmed materials synthesis with DNA". *Chemical Reviews* **99**, 1849-1862 (1999).

[12] Park, S. Y., Lytton-Jean, A. K., Lee, B., Weigand, S., Schatz, G. C. & Mirkin, C. A. "DNA-programmable nanoparticle crystallization". *Nature* **451**, 553-556 (2008).

[13] Moores, A. & Goettmann, F. "The plasmon band in noble metal nanoparticles: an introduction to theory and applications". *New Journal of Chemistry* **30**, 1121-1132 (2006).

[14] Kelly, K. L., Coronado, E., Zhao, L. L. & Schatz, G. C. (2003).

[15] Petryayeva, E. & Krull, U. J. "Localized surface plasmon resonance: Nanostructures, bioassays and biosensing—A review". *Analytica chimica acta* **706**, 8-24 (2011).

[16] An, H. & Jin, B. "Prospects of nanoparticle–DNA binding and its implications in medical biotechnology". *Biotechnology advances* **30**, 1721-1732 (2012).

[17] Kemper, B., Zengerling, L., Spitzer, D., Otter, R., Bauer, T. & Besenius, P. "Kinetically controlled stepwise self-assembly of AuI-metallopeptides in water". *Journal of the American Chemical Society* **140**, 534-537 (2018).

[18] Dixon, J. M. & Egusa, S. "Conformational change-induced fluorescence of bovine serum albumin–gold complexes". *Journal of the American Chemical Society* **140**, 2265-2271 (2018).

[19] Ye, R., Zhukhovitskiy, A. V., Kazantsev, R. V., Fakra, S. C.,

Wickemeyer, B. B., Toste, F. D. & Somorjai, G. A. "Supported Au nanoparticles with N-heterocyclic carbene ligands as active and stable heterogeneous catalysts for lactonization". *Journal of the American Chemical Society* **140**, 4144-4149 (2018).

[20] Liu, J. "Adsorption of DNA onto gold nanoparticles and graphene oxide: surface science and applications". *Physical chemistry chemical physics* **14**, 10485-10496 (2012).

[21] Koo, K. M., Sina, A. A., Carrascosa, L. G., Shiddiky, M. J. & Trau, M. "DNA–bare gold affinity interactions: mechanism and applications in biosensing". *Analytical Methods* **7**, 7042-7054 (2015).

[22] Storhoff, J. J., Elghanian, R., Mirkin, C. A. & Letsinger, R. L. "Sequence-dependent stability of DNA-modified gold nanoparticles". *Langmuir* **18**, 6666-6670 (2002).

[23] Yang, J., Lee, J. Y., Too, H.-P., Chow, G.-M. & Gan, L. M. "Single stranded DNA stabilization and assembly of Au nanoparticles of different sizes". *Chemical physics* **323**, 304-312 (2006).

[24] Li, H. & Rothberg, L. "Colorimetric detection of DNA sequences based on electrostatic interactions with unmodified gold nanoparticles". *Proceedings of the National Academy of Sciences* **101**, 14036-14039 (2004).

[25] Carnerero, J. M., Jimenez - Ruiz, A., Castillo, P. M. & Prado - Gotor, R. "Covalent and Non - Covalent DNA - Gold - Nanoparticle Interactions: New Avenues of Research". *ChemPhysChem* **18**, 17-33

(2017).

[26] Gisbert - Quilis, P., Masetti, M., Morla - Folch, J., Fitzgerald, J. M., Pazos - Perez, N., Garcia - Rico, E., Giannini, V., Alvarez - Puebla, R. A. & Guerrini, L. "The structure of short and genomic DNA at the interparticle junctions of cationic nanoparticles". *Advanced Materials Interfaces* **4**, 1700724 (2017).

[27] Kim, H. J., Roh, Y. & Hong, B. "Controlled gold nanoparticle assembly on DNA molecule as template for nanowire formation". *Journal of Vacuum Science & Technology A: Vacuum, Surfaces, and Films* **24**, 1327-1331 (2006).

[28] Warner, M. G. & Hutchison, J. E. "Linear assemblies of nanoparticles electrostatically organized on DNA scaffolds". *Nature materials* **2**, 272-277 (2003).

[29] Chao, J., Zhang, Y., Zhu, D., Liu, B., Cui, C., Su, S., Fan, C. & Wang, L. "Hetero-assembly of gold nanoparticles on a DNA origami template". *Science China Chemistry* **59**, 730-734 (2016).

[30] Mahato, R. I. & Kim, S. W. *Pharmaceutical perspectives of nucleic acid-based therapy*. (CRC Press, 2002).

[31] Iwataki, T., Yoshikawa, K., Kidoaki, S., Umeno, D., Kiji, M. & Maeda, M. "Cooperativity vs. phase transition in a giant single DNA molecule". *Journal of the American Chemical Society* **122**, 9891-9896 (2000).

[32] Schiessel, H. "The physics of chromatin". *Journal of Physics:*

Condensed Matter **15**, R699 (2003).

[33] Nozaki, T., Imai, R., Tanbo, M., Nagashima, R., Tamura, S., Tani, T., Joti, Y., Tomita, M., Hibino, K. & Kanemaki, M. T. "Dynamic organization of chromatin domains revealed by super-resolution live-cell imaging". *Molecular cell* **67**, 282-293. e287 (2017).

[34] Cortini, R., Barbi, M., Caré, B. R., Lavelle, C., Lesne, A., Mozziconacci, J. & Victor, J.-M. "The physics of epigenetics". *Reviews of Modern Physics* **88**, 025002 (2016).

[35] Lee, P. & Meisel, D. "Adsorption and surface-enhanced Raman of dyes on silver and gold sols". *The Journal of Physical Chemistry* **86**, 3391-3395 (1982).

[36] Liu, X., Atwater, M., Wang, J. & Huo, Q. "Extinction coefficient of gold nanoparticles with different sizes and different capping ligands". *Colloids and Surfaces B: Biointerfaces* **58**, 3-7 (2007).

[37] Tongu, C., Kenmotsu, T., Yoshikawa, Y., Zinchenko, A., Chen, N. & Yoshikawa, K. "Divalent cation shrinks DNA but inhibits its compaction with trivalent cation". *The Journal of chemical physics* **144**, 205101 (2016).

[38] Zinchenko, A. A., Luckel, F. & Yoshikawa, K. "Transcription of giant DNA complexed with cationic nanoparticles as a simple model of chromatin". *Biophysical journal* **92**, 1318-1325 (2007).

[39] Bloomfield, V. A. "DNA condensation". *Current opinion in structural biology* **6**, 334-341 (1996).

[40] Wang, M. C. & Uhlenbeck, G. E. "On the theory of the Brownian motion II". *Reviews of modern physics* **17**, 323 (1945).

[41] Marko, J. F. & Siggia, E. D. "Stretching dna". *Macromolecules* **28**, 8759-8770 (1995).

[42] Wang, M. D., Yin, H., Landick, R., Gelles, J. & Block, S. M. "Stretching DNA with optical tweezers". *Biophysical journal* **72**, 1335-1346 (1997).

[43] Appleyard, D. C., Vandermeulen, K., Lee, H. & Lang, M. J. "Optical trapping for undergraduates". *American journal of physics* **75**, 5-14 (2007).

[44] Ghosh, S. K. & Pal, T. "Interparticle coupling effect on the surface plasmon resonance of gold nanoparticles: from theory to applications". *Chemical reviews* **107**, 4797-4862 (2007).

[45] Lopatina, L. I., Karpushkin, E. A., Zinchenko, A. & Sergeyev, V. G. "Decoration of DNA scaffold by gold nanoparticles formed in aqueous solutions". *Mendeleev Communications* **26**, 291-292 (2016).

[46] Chen, Z., Liu, C., Cao, F., Ren, J. & Qu, X. "DNA metallization: principles, methods, structures, and applications". *Chemical Society Reviews* **47**, 4017-4072 (2018).

[47] Li, H. & Rothberg, L. J. "Label-free colorimetric detection of specific sequences in genomic DNA amplified by the polymerase chain reaction". *Journal of the American Chemical Society* **126**, 10958-10961 (2004).

[48] Yang, J., Pong, B.-K., Lee, J. Y. & Too, H.-P. "Dissociation of double-stranded DNA by small metal nanoparticles". *Journal of inorganic biochemistry* **101**, 824-830 (2007).

[49] Sun, L., Zhang, Z., Wang, S., Zhang, J., Li, H., Ren, L., Weng, J. & Zhang, Q. "Effect of pH on the interaction of gold nanoparticles with DNA and application in the detection of human p53 gene mutation". *Nanoscale research letters* **4**, 216-220 (2009).

[50] Zhang, X., Servos, M. R. & Liu, J. "Surface science of DNA adsorption onto citrate-capped gold nanoparticles". *Langmuir* **28**, 3896-3902 (2012).

[51] Han, G., Martin, C. T. & Rotello, V. M. "Stability of gold nanoparticle - bound DNA toward biological, physical, and chemical agents". *Chemical biology & drug design* **67**, 78-82 (2006).

[52] Fu, R., Wang, C., Zhuang, J. & Yang, W. "Adsorption and desorption of DNA on bovine serum albumin modified gold nanoparticles". *Colloids and surfaces A: physicochemical and engineering aspects* **444**, 326-329 (2014).

[53] Carnerero, J. M., Jimenez-Ruiz, A., Grueso, E. M. & Prado-Gotor, R. "Understanding and improving aggregated gold nanoparticle/dsDNA interactions by molecular spectroscopy and deconvolution methods". *Physical Chemistry Chemical Physics* **19**, 16113-16123 (2017).

[54] Rosa, M., Dias, R., da Graça Miguel, M. & Lindman, B. "DNA–cationic surfactant interactions are different for double-and single-

stranded DNA". *Biomacromolecules* **6**, 2164-2171 (2005).

[55] Heath, P. J., Clendenning, J. B., Fujimoto, B. S. & Schurr, M. J. "Effect of bending strain on the torsion elastic constant of DNA". *Journal of molecular biology* **260**, 718-730 (1996).

Chapter 3

Transitions among cracking, peeling and homogenization on drying of an aqueous solution containing glucose and starch

3.1 Introduction

It is well known that drying of polymer and colloid solutions on a solid substrate is frequently rather inhomogeneous, and is accompanied by cracking[1-8], layering[9-19], patterning[20] such as in the coffee-ring effect[21-23] and whole morphological change[24], etc. Studies on the formation of a rich variety of cracking patterns and their propagation have attracted considerable interest in the natural sciences[1-7]. In these

studies, it has been argued that cracking is induced by a tensile stress along the lateral direction through drying process. On the other hand, the appearance of a skin layer, or stratification, is a representative issue of inhomogenization, or segregation, and is rather familiar in daily life, such as in paints, cosmetics, glues, etc. Several experimental[12, 19, 25] and theoretical[9, 10, 15, 17, 18] studies have examined stratification in drying films. In many cases of stratification, films are formed from a colloidal solution with a volatile liquid. For a mixed solution with large and small particles, stratification with the small particles on the surface is fairly common[11, 13, 14, 26-28]. However, recent studies have indicated that large colloidal particles can form surface stratification under certain conditions of colloidal interaction[18, 29]. Concerning the phenomenon of stratification, peeling of a top layer occurs as a result of stratification under some conditions. However, to the best of our knowledge, there have been few studies on the formation of a peeling layer accompanied by stratification. In the present study, we observed the transition between cracking and peeling induced by drying of a mixed aqueous solution caused by a change in the compositions of glucose and starch.

3.2 Experimental Methods

Analytical-grade D-glucose (hereafter, glucose), potato starch and dimethyl sulfoxide-D6 (D_6-DMSO) were purchased from Wako Pure Chemical Industries (Osaka, Japan). Starch is a polymer that results from the dehydration of monomer glucose molecules. Thus, in the present study, we used a monomer and polymer with essentially the same chemical composition, by minimizing the influence of chemical properties, such as hydrophobicity and electronic charge. We prepared the aqueous solution by the addition of 20 g of glucose and starch, at various ratio, to 8g of deionized pure water. After mechanical agitation, the solution was transferred on to a glass petri dish with the diameter of 6 cm. Then, the solution was stood still for evaporation under room temperature around 20℃ with the humidity of around 60%.

3.3 Results and Discussion

Figure 3.1 exemplifies the change in the drying pattern for an aqueous solution containing glucose and starch at different glucose contents: $\alpha = [Glucose]/([Glucose] + [Starch])$, where [**] denotes the weight of the chemicals. In the experiments, $[Glucose] + [Starch]$ and $[Water]$ were fixed at 20g and 8g, respectively. The drying pattern changed from cracking within the two-dimensional film to peeling of the upper layer with an increase in the glucose content, α. With a further increase in α, the drying layer changes to a homogenous state. All of the experiments were performed at room temperature (20 ± 3°C) under a humidity of 40 ± 20%, and the aqueous solution was allowed to stand for 24 hours for the drying process. It may be apparent that the appearance of homogeneous state is attributable to the smaller content of the polymer, *i.e.*, starch, in the solution. Thus, in the following we would like to focus our attention on the occurrence of cracking and peeling, and on the transition between them.

To gain insight into the peeling phenomenon that accompanies a change in the chemical composition, we carried out ^{1}H NMR measurements at 400 MHz with a Bruker Ascend 400 spectrometer. Figure 3.2 exemplifies the ^{1}H NMR spectra of D_6-DMSO solutions prepared by dissolving solid samples obtained from the peeling and bottom layers; 10 mg of the dried sample was dissolved in 1 mL D_6-DMSO. In the figure, the chemical shift is calibrated by taking the ^{1}H signal as $\delta = 2.50$ ppm for the ^{1}H signal of the D_6-DMSO sample (residual proton). From the integration of each ^{1}H signal, we evaluated the relative amounts of glucose, starch and water. Table 3.1 shows

the weight ratios of glucose, starch and water obtained from the ^{1}H NMR observations for $\alpha = [Glucose]/([Glucose] + [Starch]) \approx 0.4$. in 1 mL D6-DMSO. For comparison, in the 3rd and 4th layers of Figure 3.2, pure samples of glucose and starch measured in D_6-DMSO solution are also shown. The change in the relative contents of glucose and starch indicates that the peeling layer is rich in glucose. In other words, the gradual decrease in water content in the upper portion due to evaporation causes the transfer of water together with glucose toward the upper part. On the other hand, the migration ratio of starch, as a high molecular weight polymer, is apparently smaller than those of water and glucose. Thus, the increase of the starch content in the bottom layer is attributable to the upward transfer of water and glucose and additionally to the effect of precipitation of granules of starch caused by the effect of gravity. Based on the above observation of peeling with a change in the chemical composition that accompanies the drying process, we propose a peeling mechanism as depicted schematically in Figure 3.3, which also shows the mechanism for the cracking phenomenon.

Both the cracking and peeling seen with drying are expected to be caused by gelation/solidification with the drying process. It is well known that aqueous solutions of starch undergo a transition from isotropic auqeous phase to a solidic phase with characteristics that can be described as a first-order phase transition[30-35]. Our chemical system consists of three chemical variables: water, starch, and glucose. Among these, the total amount of water decreases with time during the drying process. On the other hand, the total amounts of starch and glucose are constant. As another important physico-chemical property, the diffusion kinetics of water and glucose influence each molecule. For example, when there is a spatial gradient of glucose, water

molecules tend to migrate toward the glucose-rich region due to osmotic pressure. In contrast, starch is expected to be only minimally affected by diffusion and also to have a much weaker effect on the diffusive transport of water. While keeping in mind these characteristics of an aqueous solution containing glucose and starch, we propose a difference in the mechanisms of cracking and peeling, as shown schematically in Figure 3.3. In cracking, as water evaporates from the free surface, the thickness of the solution decreases, i.e., the concentrations of both glucose and starch increase with time. As a result, starch undergoes a transition to a solidic phase due to hard entanglement of the polymer chains of starch. If this transition exhibits behavior something like spinodal decomposition, the solid-like sheet must be destroyed, and the dry sheet undergoes cracking. For peeling observed with drying of an aqueous solution rich in glucose, evaporation from the surface layer causes a significant increase in the glucose content just beneath the surface layer. This may cause the solidification or crystallization of glucose, which, in turn, expels water molecules downward. Through this process, a water-rich layer would be generated just below the drying layer at the surface and, as a result, peeling of a thin layer would be induced.

3.4 Numerical Modeling

To examine the proposed mechanism of the transition between cracking and peeling as exemplified in Figure. 3.1, we performed a numerical simulation by using a simple nonlinear partial differential equation. We adapted a model equation similar to that in a past study, which was used to explain the segregation of large and small colloid particles between upper and lower layers under drying[10]. We consider a model with just a single variable, Φ, which roughly corresponds to the content of glucose. To capture the essential features of the observed phenomenon, we assume that the content of starch is almost constant and that water is eliminated from the surface through evaporation under the simple assumption of linear increase of Φ with time. Here, it is noted that an increase in Φ corresponds to a decrease in water content. For simplicity, we use the one-dimensional diffusion equation $\Phi = \Phi(z,t)$ for $0 < h \leq 1$.

$$\frac{\partial \Phi}{\partial t} = \frac{\partial}{\partial t}\left[D(\Phi)\frac{\partial \Phi}{\partial z}\right] + Flux(z = h) \tag{3.1}$$

To take into account the effect of squeezing of water toward the inner region caused by the solidification/ crystallization of glucose near the surface, we assume that the phenomenological diffusion constant $D(\Phi)$ on the above equation will become negative for relatively large values of Φ, *i.e.*, for a relatively low water content. To provide such a condition for the equation with tuning of the minimum number of parameters, we choose a parabolic approximation for $D(\Phi)$ [36]:

$$D(\Phi) = 0.5\Phi^2 - 0.68\Phi + a \tag{3.2}$$

By taking a to be 0.23, we obtained the change in the profile of Φ over time, as shown in Figure 3.4(b), being corresponding to the phenomenon of peeling. For comparison, numerical result by taking a constant value of *D*, *i.e.*, $D(\Phi)$ = 0.23 (constant) is shown in Fig.3.4(a), corresponding to the drying process accompanied by thining of the whole layer. It is regarded that such drying process may cause cracking. In these calculations, we adapted the spatial finite-difference method with 11 points along the z axis (vertical axis). For the time-dependent changes in Figure 3.4, we have shown the profile under the condition of fixed integrated value of Φ for z = [0 , h], where $0 < h \leq 1$. Thus, the decreases of the surface height or depth z is roughly correspond to the thinning of the whole layer owe to the water evaporation. The boundary condition for the outflux of water, $Flux(z = h)$ at the surface of the drying layer, was taken to be 0.00082 for a single time-step of the finite time difference in the simulation. In addition, to take in account of the effect owe to a "soft" boundary between the drying solution and gas phases, outflux at the depth of 0.1 from the outer surface was also adapted with the half value of that at the outer surface (by taking the outflux of 0.00082 per each two time-steps). Figure 3.4 shows that the numerical results reproduce the essential aspect of the experimental observation, in spite of the rough assumption of the numerical model. Here, it should be noted that additional considerations on the physical strain, nonlinear property of elasticity and surface tension are necessary to interpret the mechanical instability to induce cracking and peeling. Nevertheless, summarizing the above discussions, it would be concluded that the apparent negative diffusion of water molecules, or squeezing of water, for the solution condition with reltively large value of Φ, induced by the solidification transition on the

region near the surface generates the peeling phenomenon. Although our theoretical model and also experimental observation is primitive, the present study may stimulate the future development of a more detailed theory together with the additional experiments.

3.5 Conclusions

A morphological transition was observed in the drying of an aqueous solution containing glucose and starch, which are the monomer and polymer of the same chemical composite. With an increase in the glucose content, the sample exhibits a change from cracking of a 2-dimensional (2D) layer to peeling from the bottom layer. With a further increase in glucose, a 2D homogenous layer is generated. A chemical analysis revealed that the peeling film and remaining bottom layer are rich in glucose and starch, respectively. Regarding the mechanism of the transition between cracking and peeling, we propose a phenomenological nonlinear diffusion equation that includes the effect of solidification with starch polymers. The numerical results with this diffusion equation reproduce the essential features of the transition of the drying layer.

3.6 Supporting Information

Detailed information on the numerical simulation:

In the calculation, for simplification we adapted the spatial finite-difference method with 11 points along the z axis (vertical axis). The time step was taken as Δt=1. The boundary condition caused by the outflux of water, $Flux(z = h)$, was taken as an increase of Φ at the outer surface with the value of 0.00082 at $z = h$ for each single time-step of the finite time difference in the simulation. In addition, to take in account of the effect owe to a "soft" boundary between the drying solution and gas phases, outflux at $z = h - 0.1$ was also adapted with the half value of that at $z = h$ (by taking the outflux of 0.00082 per each two time-steps).

Dependences of $D(\Phi)$ on Φ adapted in the numerical simulation are schematically depicted as in Figure S3.1. We have confirmed that the appearance of the peeling layer is caused only under the condition with partially negative value on D, as exemplified in (b).This work was partly supported by JSPS KAKENHI Grant Number JP20H01877. We would like to thank Dr. K. Sadakane for the useful suggestion.

3.7 Acknowledgments

This work was partly supported by JSPS KAKENHI Grant Number JP20H01877. We would like to thank Dr. K. Sadakane for the useful suggestion.

Table 3.1 Chemical composition of the initial solution, and dried states as a peeling film and bottom layer after drying for 24 hours, evaluated from the NMR measurement.

		Glucose	Starch	Water
Initial Solution	Homogeneous Liq	0.29	0.42	0.29
After 24 hours	Peeling film	0.45	0.48	0.07
	Bottom layer	0.18	0.71	0.11

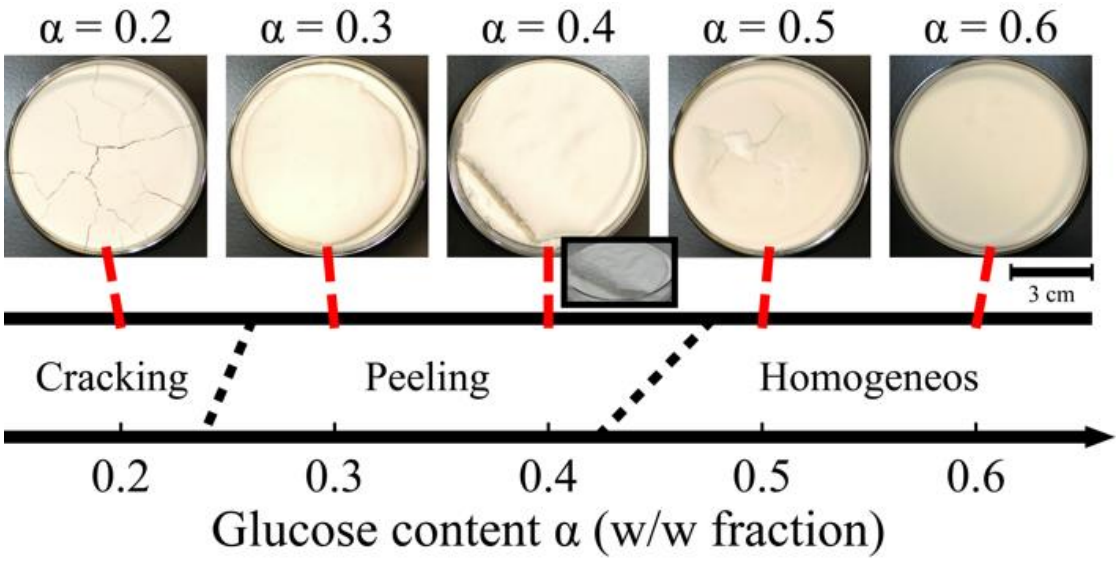

Figure 3.1 Morphological change in the dried state for an aqueous solution containing glucose and starch. The weights of [Glucose]+[Starch] and [Water] were fixed at 20g and 8g, respectively. $\alpha(\mathrm{g/g}) = [Glucose]/([Glucose] + [Starch])$

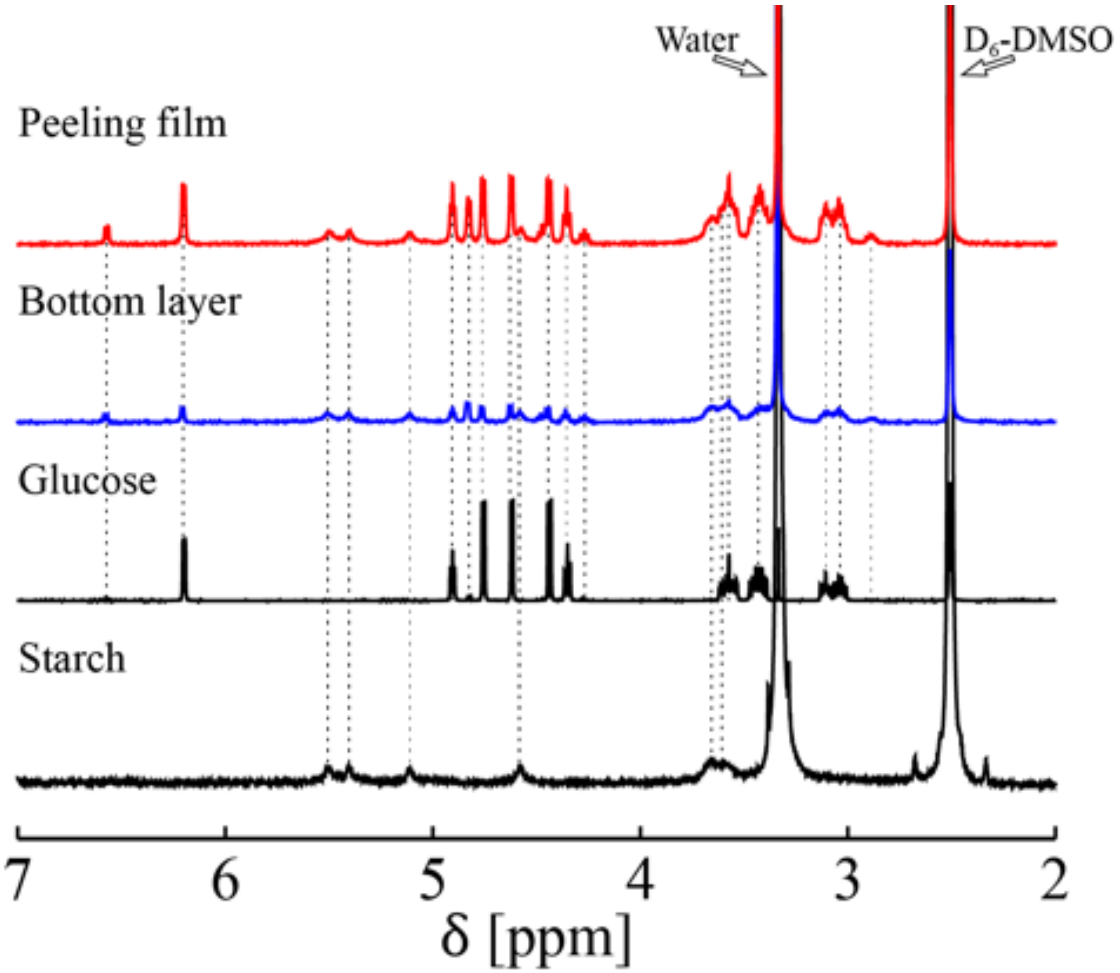

Figure 3.2 [1]H NMR spectra of peeling film, bottom layer, glucose and starch (400 MHz, D6-DMSO, [Glucose] = 8g; [Starch] = 12g; [Water] = 8g, α = 0.4).

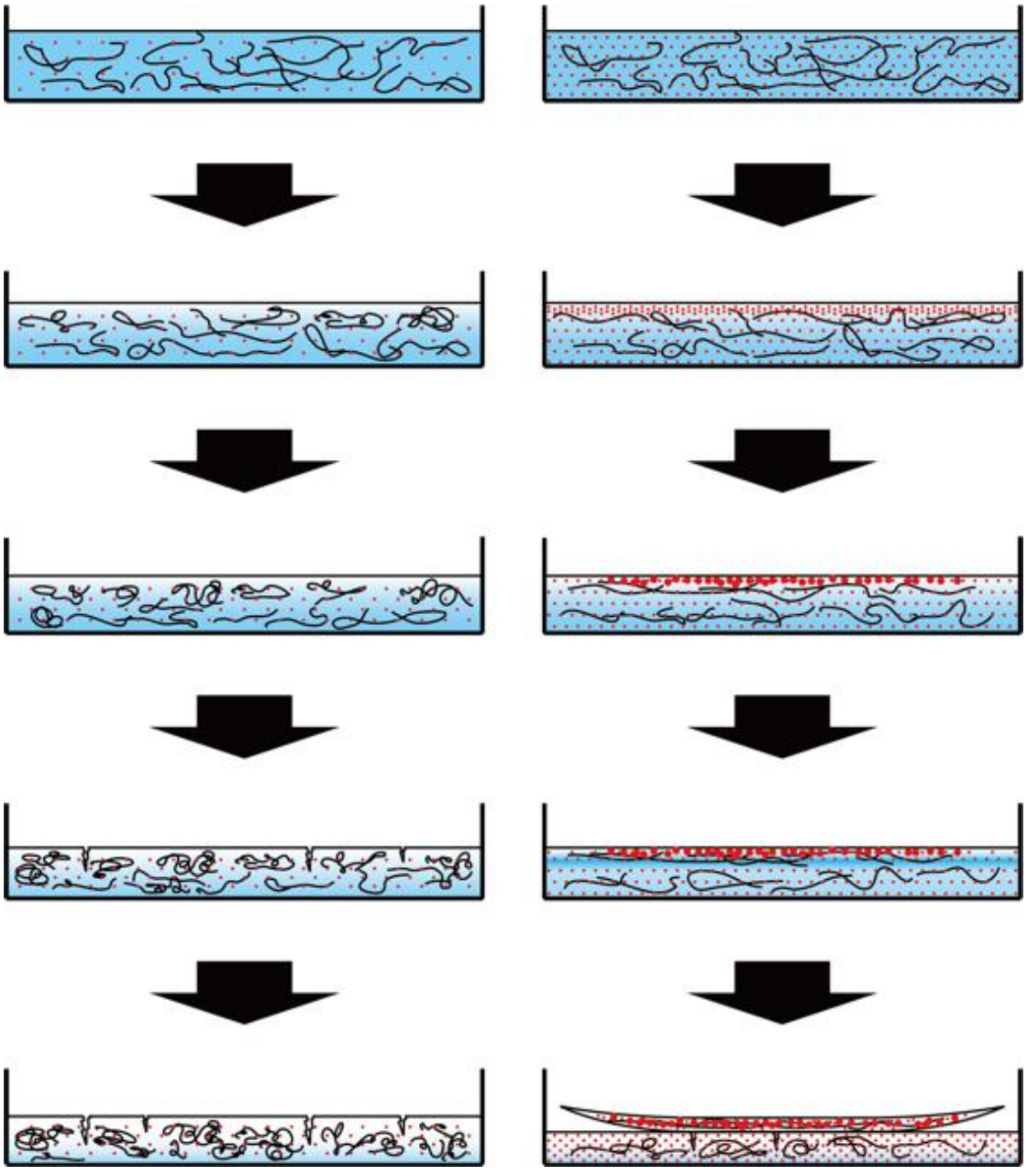

Figure 3.3 Schematic representation of the drying processes at different glucose contents (see Fig. 3.1). (a): cracking at a low glucose content; (b): peeling at a higher glucose content.

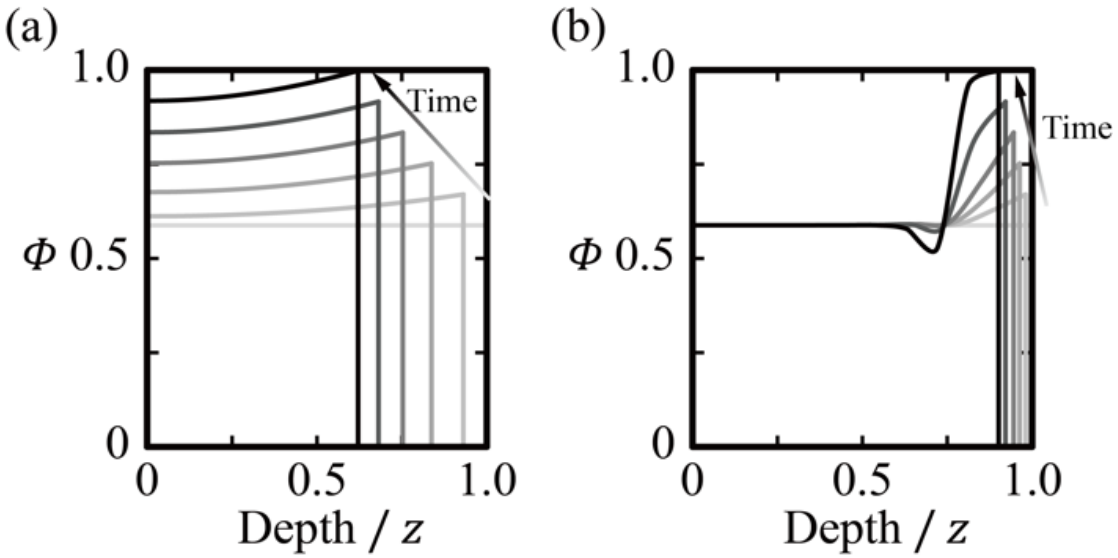

Figure 3.4 Numerical modeling of the time development of drying for an aqueous solution. (a) and (b) correspond to lower and higher glucose contents, respectively.

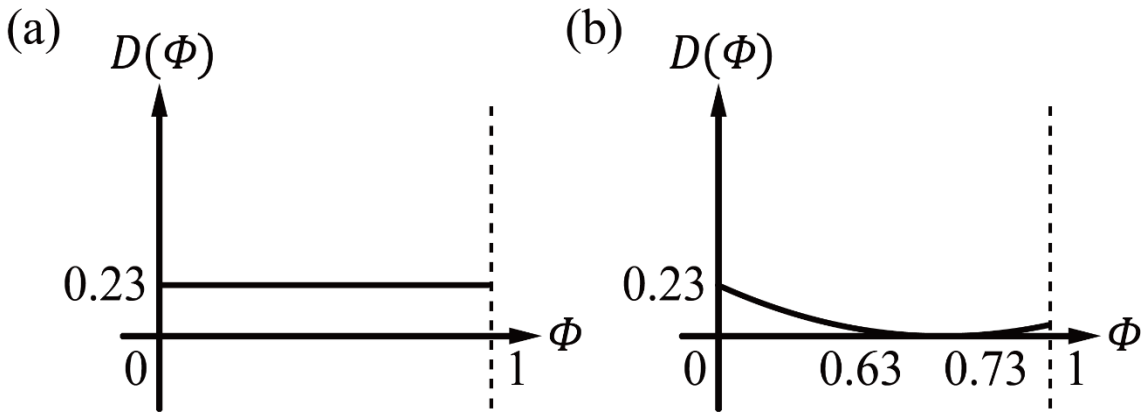

Figure S3.1 Φ dependence of $D(\Phi)$. (a) and (b) are the effective diffusion constants depending on Φ, adapted in the present simulation. In (b), $D(\Phi)$ exhibits small negative value between 0.63 and 0.73.

Referenses

[1] Griffith, A. A. "The phenomena of rupture and flow in solids". *Trans. Roy. Soc. Lond. Ser. A* **221**, 163-198 (1921).

[2] Irwin, G. R. "Analysis of Stresses and Strains near the End of a Crack Traversing a Plate". *Journal of Applied Mechanics-Transactions of the ASME* **24**, 361-364 (1957).

[3] Yuse, A. & Sano, M. "Transition between crack patterns in quenched glass plates". *Nature* **362**, 329 (1993).

[4] Nakahara, A. & Matsuo, Y. "Imprinting memory into paste and its visualization as crack patterns in drying process". *Journal of the Physical Society of Japan* **74**, 1362-1365 (2005).

[5] Goehring, L. & Morris, S. W. "Cracking mud, freezing dirt, and breaking rocks". *Physics Today* **67**, 39-44 (2014).

[6] Cho, M. R., Jung, J. H., key Seo, M., Cho, S. U., Kim, Y. D., Lee, J. H., Kim, Y. S., Kim, P., Hone, J. & Ihm, J. "Universality of periodicity as revealed from interlayer-mediated cracks". *Scientific reports* **7**, 43400 (2017).

[7] Cho, H. J. & Datta, S. S. "Scaling Law for Cracking in Shrinkable Granular Packings". *Physical Review Letters* **123** (2019).

[8] Tomar, B. S., Shahin, A. & Tirumkudulu, M. S. "Cracking in drying films of polymer solutions". *Soft Matter* **16**, 3476-3484 (2020).

[9] de Gennes, P. G. "Solvent evaporation of spin cast films: “crust”

effects". *The European Physical Journal E* **7**, 31-34 (2002).

[10] Okuzono, T., Ozawa, K. & Doi, M. "Simple model of skin formation caused by solvent evaporation in polymer solutions". *Phys Rev Lett* **97**, 136103 (2006).

[11] Nikiforow, I., Adams, J., Konig, A. M., Langhoff, A., Pohl, K., Turshatov, A. & Johannsmann, D. "Self-stratification during film formation from latex blends driven by differences in collective diffusivity". *Langmuir* **26**, 13162-13167 (2010).

[12] Shimokawa, Y., Kajiya, T., Sakai, K. & Doi, M. "Measurement of the skin layer in the drying process of a polymer solution". *Phys Rev E Stat Nonlin Soft Matter Phys* **84**, 051803 (2011).

[13] Trueman, R. E., Lago Domingues, E., Emmett, S. N., Murray, M. W., Keddie, J. L. & Routh, A. F. "Autostratification in drying colloidal dispersions: experimental investigations". *Langmuir* **28**, 3420-3428 (2012).

[14] Trueman, R. E., Lago Domingues, E., Emmett, S. N., Murray, M. W. & Routh, A. F. "Auto-stratification in drying colloidal dispersions: a diffusive model". *J Colloid Interface Sci* **377**, 207-212 (2012).

[15] Fortini, A., Martin-Fabiani, I., De La Haye, J. L., Dugas, P. Y., Lansalot, M., D'Agosto, F., Bourgeat-Lami, E., Keddie, J. L. & Sear, R. P. "Dynamic Stratification in Drying Films of Colloidal Mixtures". *Phys Rev Lett* **116**, 118301 (2016).

[16] Khodaparast, S., Boulogne, F., Poulard, C. & Stone, H. A. "Water-

based peeling of thin hydrophobic films". *Physical review letters* **119**, 154502 (2017).

[17] Sear, R. P. & Warren, P. B. "Diffusiophoresis in nonadsorbing polymer solutions: The Asakura-Oosawa model and stratification in drying films". *Phys Rev E* **96**, 062602 (2017).

[18] Zhou, J., Jiang, Y. & Doi, M. "Cross Interaction Drives Stratification in Drying Film of Binary Colloidal Mixtures". *Phys Rev Lett* **118**, 108002 (2017).

[19] De Gennes, P.-G., Brochard-Wyart, F. & Quéré, D. *Capillarity and wetting phenomena: drops, bubbles, pearls, waves*. (Springer Science & Business Media, 2013).

[20] Schulz, M. & Keddie, J. L. "A critical and quantitative review of the stratification of particles during the drying of colloidal films". *Soft Matter* **14**, 6181-6197 (2018).

[21] Deegan, R. D., Bakajin, O., Dupont, T. F., Huber, G., Nagel, S. R. & Witten, T. A. "Capillary flow as the cause of ring stains from dried liquid drops". *Nature* **389**, 827 (1997).

[22] Chen, Y. J., Suzuki, K. & Yoshikawa, K. "Self-organized target and spiral patterns through the "coffee ring" effect". *J Chem Phys* **143**, 084702 (2015).

[23] Devineau, S., Anyfantakis, M., Marichal, L., Kiger, L., Morel, M., Rudiuk, S. & Baigl, D. "Protein Adsorption and Reorganization on Nanoparticles Probed by the Coffee-Ring Effect: Application to Single

Point Mutation Detection". *J Am Chem Soc* **138**, 11623-11632 (2016).

[24] Khoozani, A. A., Bekhit, A. E. A. & Birch, J. "Effects of different drying conditions on the starch content, thermal properties and some of the physicochemical parameters of whole green banana flour". *Int J Biol Macromol* **130**, 938-946 (2019).

[25] Samanta, A. & Bordes, R. "On the effect of particle surface chemistry in film stratification and morphology regulation". *Soft Matter* **16**, 6371-6378 (2020).

[26] Howard, M. P., Nikoubashman, A. & Panagiotopoulos, A. Z. "Stratification Dynamics in Drying Colloidal Mixtures". *Langmuir* **33**, 3685-3693 (2017).

[27] Tang, Y., Grest, G. S. & Cheng, S. "Stratification of drying particle suspensions: Comparison of implicit and explicit solvent simulations". *J Chem Phys* **150**, 224901 (2019).

[28] Makepeace, D. K., Fortini, A., Markov, A., Locatelli, P., Lindsay, C., Moorhouse, S., Lind, R., Sear, R. P. & Keddie, J. L. "Stratification in binary colloidal polymer films: experiment and simulations". *Soft Matter* **13**, 6969-6980 (2017).

[29] Cheng, S. & Grest, G. S. "Dispersing Nanoparticles in a Polymer Film via Solvent Evaporation". *ACS Macro Letters* **5**, 694-698 (2016).

[30] Donovan, J. W. "Phase transitions of the starch–water system". *Biopolymers: Original Research on Biomolecules* **18**, 263-275 (1979).

[31] Donovan, J. & Mapes, C. "Multiple phase transitions of starches and

Nägeli amylodextrins". *Starch - Stärke* **32**, 190-193 (1980).

[32] Wang, S. S., Chiang, W., Zhao, B., Zheng, X. & Kim, I. H. "Experimental analysis and computer simulation of starch - water interactions during phase transition". *Journal of food science* **56**, 121-124 (1991).

[33] Nishiyama, Y., Putaux, J. L., Montesanti, N., Hazemann, J. L. & Rochas, C. "B-->A Allomorphic transition in native starch and amylose spherocrystals monitored by in situ synchrotron X-ray diffraction". *Biomacromolecules* **11**, 76-87 (2010).

[34] van der Sman, R. G. M. & Meinders, M. B. J. "Prediction of the state diagram of starch water mixtures using the Flory–Huggins free volume theory". *Soft Matter* **7**, 429-442 (2011).

[35] Wang, S. & Copeland, L. "Phase transitions of pea starch over a wide range of water content". *J Agric Food Chem* **60**, 6439-6446 (2012).

[36] Miranville, A. "The Cahn–Hilliard equation and some of its variants". *AIMS Mathematics* **2**, 479-544 (2017).

Chapter 4

Fluctuation of standing body: Large difference on the time-development between left/right and front/rear fluctuations

4.1 Introduction

Living organisms, including human, maintain their activity along time-development. Currently, time-dependent fluctuations in life matters and also alife events have been analyzed in terms of frequency analysis. Most often, FFT of the time fluctuation is performed and characteristic frequency have been deduced. When the fluctuation is generated induced by a certain outer stimulus, one can obtain the

information of phase-shift in addition to the frequency spectrum, through the calculation of complex FFT. Whereas, as for the natural fluctuation without outer stimulus it becomes almost impossible to argue the phase-shift with FFT, and usually only the power spectrum is the informational parameter on the fluctuation. The discard of the parameter of phase shift implies that the information along time-development, or difference between past and future, becomes to be completely missing state. Here, we would like to show a new methodology to abstract the information along time-axis, in other words, to evaluate the degree of symmetry breaking with respect to time arrow. We will demonstrate that such parameter of time–inversion asymmetry is useful to evaluate the hidden characteristics on the time-dependent fluctuation under thermodynamically dissipative conditions, being general for living organisms [1-5].

.

4.2 Methods

We observed fluctuation of human body with standing conditions by a balance Wii board (Nintendo Co., Ltd, Japan), which has four sensors on pressure and Bluetooth wireless system. The shifts of center of mass on body monitored by the Wii board during measurement have been send to the PC so as to store the observed data on X and Y position by the wireless system. Motion of body has been monitored by a video camera (Nikon J4) with the frame rate of 60 frames/sec. Figure 4.1 (a) and (b) shows a schematic of the standing conditions on the Wii board in the present work; the upright posture or posture with legs as front and back. We have set a Y axis as taking the same direction of line of slight and a X axis have been taken in right angle against Y axis as shown in Fig. 4.1(c). Fig. 4.1(c) also shows the directions of the front/rear and left/right directions.

4.3 Results and Discussion

Figure 4.2 shows the time-delay maps of the directions on the left/right and front/rear for several time intervals under the standing condition of both legs with eyes of a research subject opened. The time-delay maps describe a correlation between X(t) and X(t+a) with time interval, where n denotes a number of observed data. The color of the plot indicates the time of the n-th data. The results indicates that the correlations are close to unity up to 0.1 s, and decreases with time above 0.1 s for both left/right and front/rear conditions. The correlation on the case of the front/rear in Fig. 4.2 is slightly strong compared with that for the left/right. Shown in Fig. 4.3 are the time-delay maps with similar condition in Fig. 4.2, except that the research subject close own eyes. The correlations are similar trend for the cases on the left/right and front/rear. No marked difference on fluctuations are observed in the cases which the research subject open own eyes or not.

Figure 4.4 and 4.5 indicate time-delay maps on the body fluctuations with the condition, which the research subject stand with own legs as front and back and the eyes are opened or closed. Experimental results have indicated that the areas drawn by lines are larger than those for the cases in Figs. 4.3 and 4.4. This means that the correlations with the legs as front and back are weak compared with the cases of the upright posture. Especially, the time delay map of the left and right of the fluctuation of Fig. 4.5 is significantly different from the other results. The locations of each data points with short time interval, which have similar color each other, are scattered widely. We consider that the fluctuation in this case is rather large compared with those for other

cases. The typical deviations of the front/rear in Fig. 4.4 have been found in the upper part against a line of $X(t) = X(t+0.2)$. This mean that the time reversal symmetry is broken in this case. Such deviation is not observed in the standing condition which the research subject close own eyes. Thus, the condition which research's eyes is open take a decisive role to characterize the body fluctuation of the front/rear.

The analysis results of the time-delay maps show the strong correlation in the cases of the upright posture with the time intervals less than 0.1 s. However, the degree of correlations decreases in accordance with the increase of time interval. These results provide fundamental understandings on the characteristic of self-control or self-feedback mechanisms on the stability of body balance on human being. We consider that the characteristics on the stabilities of body fluctuations can adopt to control a robot so as to keep the stabilities of standing and walking states like a human being.

4.4 Conclusions

We evaluated quantitatively the fluctuations of body with several standing conditions by using an electronic balance, Wii board. The results analysis with time-delay maps show that time-inversion symmetry is broken in an apparent manner for the time scale of 0.1 s with the standing conditions of the upright posture. Whereas, the time-inversion symmetry is almost preserved for the time scale less than 0.1 s. These findings provide novel type of information embedded in the time-dependent fluctuation of a standing body, as one of the essential characteristics of a self-feedback system as in human beings.

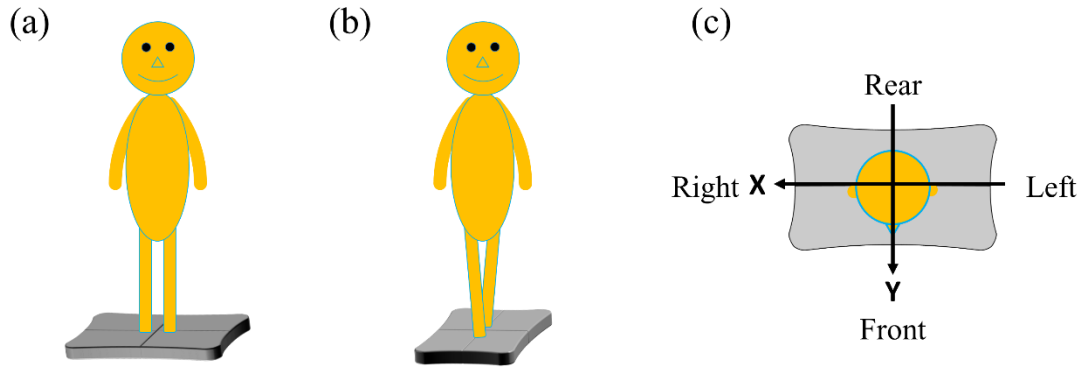

Figure 4.1 Schematics of standing conditions. (a) Standing condition on the upright posture. (b) Standing on the condition of posture with legs as front and back. (c) Directions of X-Y axis, Front/Rear and Left/Right.

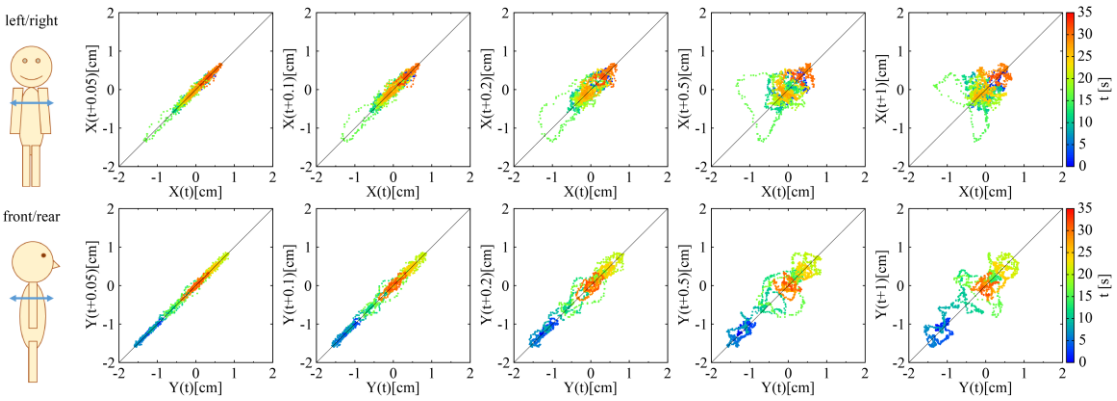

Figure 4.2 Time-delay maps on the body fluctuations in the directions of the left/right and front/rear with the subject's eyes opened. Colors express the elapsed time.

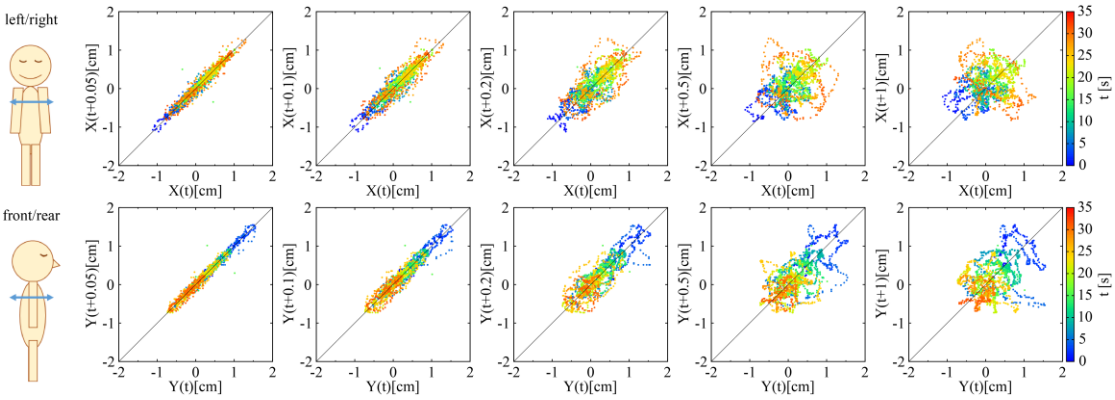

Figure 4.3 Time-delay maps on the body fluctuations in the directions of the left/right and front/rear with the subject's eyes closed. Colors express the elapsed time.

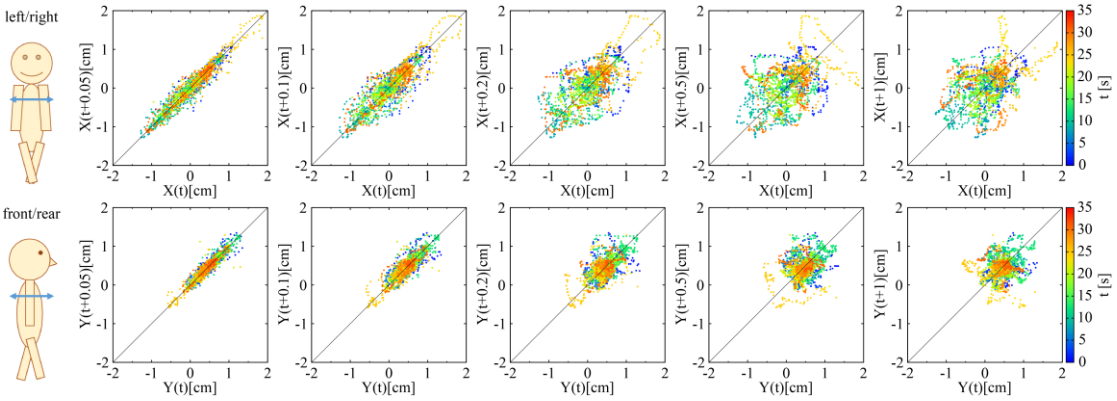

Figure 4.4 Time-delay maps on the body fluctuations in the directions of the left/right and front/rear with the legs as front and back and the subject's eyes opened. Colors express the elapsed time.

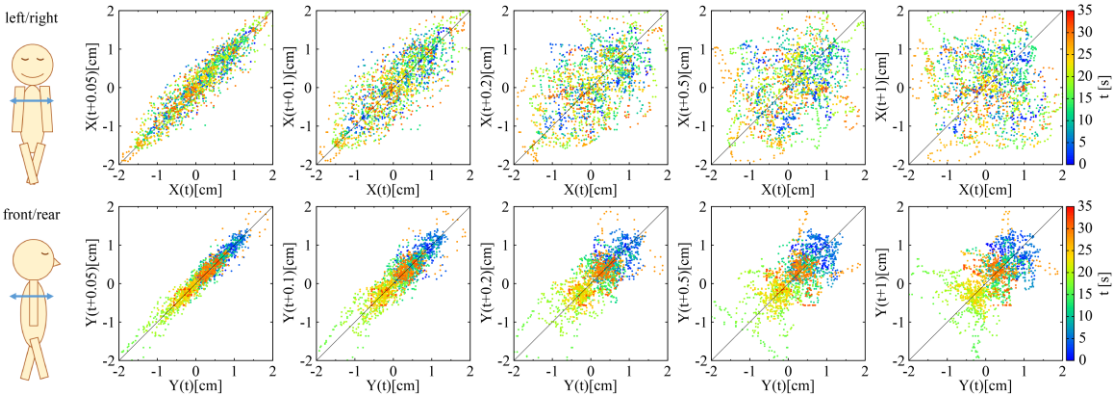

Figure 4.5 Time-delay maps on the body fluctuations in the directions of the left/right and front/rear with the legs as front and back and the subject's eyes closed. Colors express the elapsed time.

References

[1] Harada, T. & Yoshikawa, K. "Fluctuation-response relation in a rocking ratchet". *Physical Review E* **69**, 031113 (2004).

[2] Kubo, Y., Inagaki, S., Ichikawa, M. & Yoshikawa, K. "Mode bifurcation of a bouncing dumbbell with chirality". *Physical Review E* **91**, 052905 (2015).

[3] Speck, T. & Seifert, U. "The Jarzynski relation, fluctuation theorems, and stochastic thermodynamics for non-Markovian processes". *Journal of Statistical Mechanics: Theory and Experiment* **2007**, L09002 (2007).

[4] Kim, S.-Y. & Hu, B. "Bifurcations and transitions to chaos in an inverted pendulum". *Physical Review E* **58**, 3028 (1998).

[5] Kiss, P. & Jánosi, I. M. "Time-asymmetric fluctuations in the atmosphere: daily mean temperatures and total-column ozone". *Philosophical Transactions of the Royal Society A: Mathematical, Physical and Engineering Sciences* **368**, 5721-5735 (2010).

Chapter 5

General Conclusions

In this paper, we showed the results of quantifying and modeling the formation of spatiotemporal order on all length scales using experimental and theoretical methods. "Unveiling the fundamental mechanisms" in the title means exploring complex life by targeting natural phenomena that symbolically cut out the characteristics of life.

In Chapter 2, we discovered that genome-sized single-molecule DNA causes characteristic fluctuations on the order of seconds, which can be said to be relatively long for substances on the order of nanometers. Furthermore, we succeeded in numerically evaluating the viscoelastic properties of individual single DNA molecules under conditions close to in-vivo environment.

In Chapter 3, we experimentally discovered that the drying pattern shifts depending on the mixing ratio of glucose and starch. In addition, by using a mathematical model of a simple one-dimensional diffusion equation, it was clarified that the transition of the drying pattern is caused by the phase transition of glucose and water.

In Chapter 4, we analyzed the fluctuation of the body from the viewpoint of breaking the time inversion symmetry. It has become possible to numerically evaluate the information of the arrow of time, which could not be evaluated by the conventional analysis method.

Thus, in Chapters 2-4, we have extended the research to shed light on the fundamental role of the interplay with disorder and fluctuation for the generation of spatio-temporal order and also living systems, by combining the approaches of simple experiments and theoretical modeling's. Each study focuses on different phenomena, but they are the same in that they form a spatio-temporal order in a hierarchy.

Here, it may be of interesting to note that the reason for the Nobel Prize in Physics 2021 for G. Parisi is "for the discovery of the interplay of disorder and fluctuations in physical systems from atomic to planetatry scales", who got the half of the Prize in Physics (the other have was given for S. Manabe and K. Hasselmann) [1]. Although the contents of the present thesis are somewhat narrower compared to G. Parisi, i.e., from nm to meter scales, the essence of the interests resembles to his research mind. Life causes self-organizing phenomena such as rhythmic movements and pattern formation on all length scales, accompanied by the transfer of energy such as heat and light. I have shown that deeper understanding of these complex systems is obtained by combining relatively simple experimental subjects with the support of simple but fundamental theoretical modeling. Further study along such line is expected to shed light on unsolved problems in complex systems.

Referenses

[1] Nobel Prize PRESS RELEASE "The Nobel Prize in Physics 2021" (2021).

Publications

[1] Carnerero, J. M., Masuoka, S., Baba, H., Yoshikawa, Y., Prado-Gotor, R. & Yoshikawa, K. "Decorating a single giant DNA with gold nanoparticles". *RSC advances* **8**, 26571-26579 (2018).

[2] Baba, H., Takatori, S., Sadakane, K., Kenmotsu, T. & Yoshikawa, K. "Fluctuation of standing body: Large difference on the time-development between left/right and front/rear fluctuations". *2016 International Symposium on Micro-NanoMechatronics and Human Science (MHS)*, 1-5 (2016).

[3] Baba, H., Yoshioka, R., Takatori, S., Oe, Y. & Yoshikawa, K. "Transitions among Cracking, Peeling and Homogenization on Drying of an Aqueous Solution Containing Glucose and Starch". *Chemistry Letters* **50**, 1011-1014 (2021).

Acknowledgments

Firstly, I am grateful to my supervisor, Prof. Yohei Oe and second supervisors, Prof. Akihisa Shioi and Assoc. Prof. Koichiro Sadakane for useful discussions and advice for this thesis. I could not complete this dissertation without their gentle questions and suggestions for my thesis.

I express my sincere thanks to Prof. Kenichi Yoshikawa for the continuous support of my study and related research, for his patience, motivation, and immense knowledge. His guidance helped me in all the time of research and writing of this thesis. I could not have imagined having a better advisor and mentor for my study.

Besides my advisor, I am also grateful to Prof. Takahiro Kenmotsu. I am extremely thankful and indebted to him for sharing expertise, and sincere and valuable guidance and encouragement extended to me.

I would like to thank Prof. Rafael Prado-Gotor and Prof. Yuko Yoshikawa for their active discussion as a co-author.

I would like to special thank Dr. Jose Maria Carnerero, Mr. Shinsuke Masuoka and Ms. Risa Yoshioka, who actually carried out the experimental part and provided experimental data.

I would also like to thank Dr. Yue Ma who is my English adviser, and Dr. Hiroki Sakuta and Dr. Hiroshi Ueno who gave me advises about the experiment, and Takashi Nishio who is back-to-back comrade.

I would like to thank Ms. Makiko Furumoto, Secretary of the Life Physics Laboratory, for her support in various ways in conducting the research.

I would also like to take this opportunity to express gratitude to all of the laboratory members for their help and support.

Last but not least, I would like to thank my family: my parents, my brother, my sister and Dr. Satoshi Takatori for supporting me spiritually throughout writing this thesis and my life in general. I would like to extend my indebtedness to my family for their continuous and unparalleled love, understanding, support, encouragement and sacrifice throughout my study.